

000 001 Li₂: A FRAMEWORK ON DYNAMICS OF FEATURE 002 EMERGENCE AND DELAYED GENERALIZATION 003 004

005 **Anonymous authors**
006 Paper under double-blind review

007 008 ABSTRACT 009

011 While the phenomenon of grokking, i.e., delayed generalization, has been studied
012 extensively, it remains an open problem whether there is a mathematical frame-
013 work that characterizes what kind of features will emerge, how and in which con-
014 ditions it happens, and is still closely connected with the gradient dynamics of the
015 training, for complex structured inputs. We propose a novel framework, named
016 Li₂, that captures three key stages for the grokking behavior of 2-layer nonlinear
017 networks: (I) **Lazy learning**, (II) **independent feature learning** and (III) **interactive**
018 **feature learning**. At the lazy learning stage, top layer overfits to random hid-
019 den representation and the model appears to memorize. During lazy learning,
020 the *backpropagated gradient* G_F from the top layer carries information about
021 the target label, with a specific structure that enables each hidden node to learn
022 their representation *independently*. Interestingly, the independent dynamics fol-
023 lows exactly the *gradient ascent* of an energy function \mathcal{E} , and its local maxima
024 are precisely the emerging features. We study whether these local-optima induced
025 features are generalizable, their representation power, and how they change on
026 sample size, in group arithmetic tasks. When hidden nodes start to interact in the
027 later stage of learning, we provably show how G_F changes to focus on missing
028 features that need to be learned. Our study sheds lights on roles played by key hy-
029 perparameters such as weight decay, learning rate and sample sizes in grokking,
030 leads to provable scaling laws of feature emergence, memorization and general-
031 ization, and reveals the underlying cause why recent optimizers such as Muon can
032 be effective, from the first principles of gradient dynamics. Our analysis can be
033 extended to multi-layer architectures.

034 1 INTRODUCTION

035 While modern deep models such as Transformers have achieved impressive empirical performance,
036 it remains a mystery how such models acquire the knowledge during the training process. There
037 have been ongoing arguments on whether the models can truly generalize beyond what it is trained
038 on, or just memorize the dataset and performs poorly in out-of-distribution (OOD) data (Wang et al.,
039 2024b; Chu et al., 2025; Mirzadeh et al., 2024).

040 Modeling the memorization/generalization behaviors have been a goal of many works. One such
041 behavior, known as *grokking* (Power et al., 2022; Doshi et al., 2024; Nanda et al., 2023; Wang et al.,
042 2024a; Varma et al., 2023; Liu et al., 2023; Thilak et al., 2022), shows that the model initially overfits
043 to the training set, and then suddenly generalizes to unseen test samples after continuous training.
044 Many explanation exists, e.g., effective theory (Liu et al., 2022; Clauw et al., 2024), efficiency of
045 memorization and generalization circuits (Varma et al., 2023), Bayesian interpretation with weight
046 decay as prior (Millidge, 2022), etc. Most works focus on a direct explanation of its empirical
047 behaviors, or leverage property of very wide networks (Barak et al., 2022; Mohamadi et al., 2024;
048 Rubin et al., 2024), but few explores the details of the grokking learning procedure by studying the
049 gradient dynamics on the weights.

050 In this work, we propose a mathematical framework Li₂ that divides the grokking dynamics for
051 2-layer nonlinear networks into three major stages (Fig. 1). *Stage I: Lazy Learning*: when training
052 begins, the top (output) layer learns first with random features from the hidden layer, the backprop-
053 agated gradient G_F to the hidden layer is noise. *Stage II: Independent feature learning*: After that,
the weights of the output layer is no longer random, the backpropagated gradient G_F starts to carry

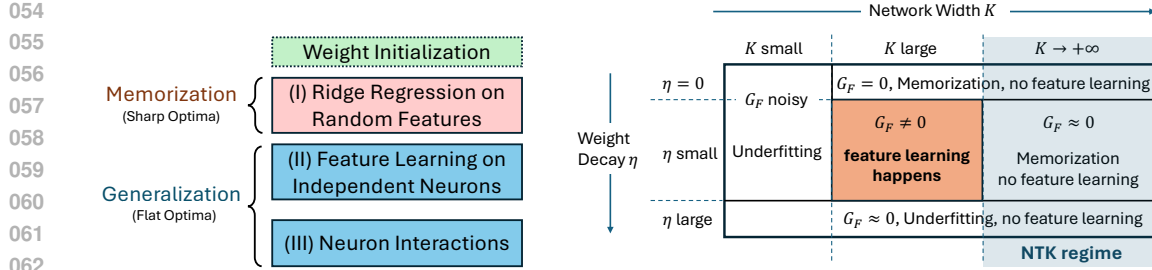


Figure 1: Overview of our framework Li_2 . **Left:** Li_2 proposes three stages of the learning process, (I) Lazy learning, (II) independent feature learning and (III) interactive feature learning, to explain the dynamics of grokking that shows the network first memorizes then generalizes. **Right:** Our analysis covers a wide range of network width K and weight decay η and demonstrates their effects on learning dynamics, including both NTK and feature learning regime. In the feature learning regime, with the help of the energy function \mathcal{E} (Thm. 1), we characterize the learned features as local maxima of \mathcal{E} (Thm. 2) and the required sample size to maintain them (Thm. 4), establishing generalization/memorization scaling laws.

information about the target in the presence of weight decay (Lemma 1), which drives the learning of hidden representations. In this stage, the backpropagated gradient of the j -th neuron (node) only depends on its own activation, triggering independent feature learning for each node. *Stage III: Interactive feature learning*: when weights in the hidden layer get updated and are no longer independent, interactions across nodes adjust the learned feature to minimize the loss.

We study each stages in detail and provide theoretical analysis. In *Stage I*, G_F carries target labels once the top layer overfits. In *Stage II*, independent feature learning follows gradient ascent of energy \mathcal{E} (Thm. 1), a nonlinear CCA. For group arithmetic, we characterize all local maxima of \mathcal{E} (Thm. 2) and show how training samples determine stability and generalizability (Thm. 4), establishing scaling laws. In *Stage III*, we prove diversity push (Thm. 6), top-down modulation (Thm. 7), and Muon’s effectiveness (Thm. 8). Experiments support our claims (Fig. 4).

Comparison with existing grokking frameworks. Our framework provides a theoretical foundation from first principles (i.e., gradient dynamics) that explains the empirical hypothesis Varma et al. (2023) that “*generalization circuits \mathcal{C}_{gen} is more efficient but learn slower than memorization circuits \mathcal{C}_{mem}* ”. Specifically, we show that the data distribution determines the optimization landscape, which in turn governs which local optima the weights converge into, which lead to the behavior of memorization or generalization. We also show that the initial memorization, or lazy learning (Stage I), has to happen before feature learning (Stage II-III), since the former provides meaningful backpropagated gradient G_F for the latter to start developing. In comparison, (Nanda et al., 2023) also provides a three stage framework of grokking, but mostly from empirical observations.

2 RELATED WORKS

Explanation of Grokking. Multiple explanations of grokking exist, e.g., competition of generalization and memorization circuits (Merrill et al., 2023), a shift from lazy to rich regimes Kumar et al. (2024), etc. Dynamics of grokking is analyzed in specific circumstance, e.g., for clustering data (Xu et al., 2023), linear network (Dominé et al., 2024), etc. In comparison, our work studies the full dynamics of feature emergence driven by backpropagation in group arithmetic tasks for deep nonlinear networks, and provide a systematic mathematical framework about what and how features emerge and a scaling law about when the transition between memorization and generalization happens.

Usage of group structure. Recent work leverages group theory to study the structure of final grokked solutions (Tian, 2025; Morwani et al., 2023; Shutman et al., 2025). None of them tackle the dynamics of grokking in the presence of the underlying structure of the data as we do.

Scaling laws of memorization and generalization. Previous works have identified scaling laws for memorization/generalization (Nguyen & Reddy, 2025; Wang et al., 2024a; Abramov et al., 2025; Doshi et al., 2023) without systematic theoretical explanation. Our work models such transitions as whether generalizable local optima remain stable under data sampling, and provide theoretical framework from first principles.

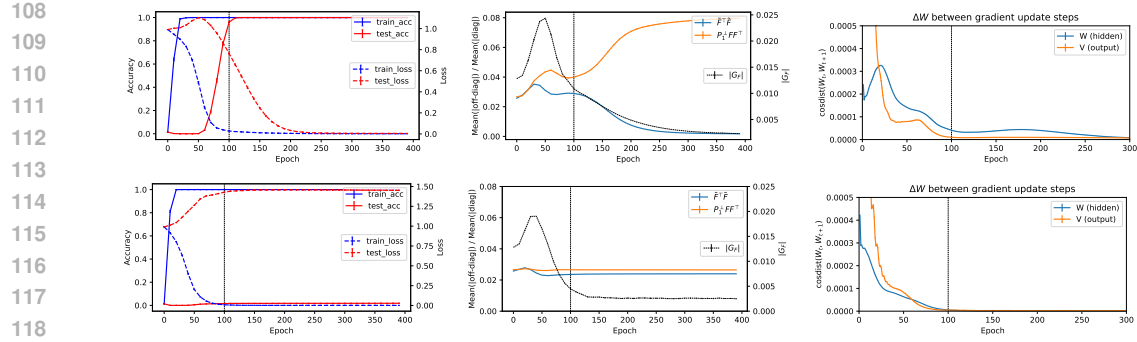


Figure 2: Grokking dynamics on modular addition task with $M = 71$, $K = 2048$, $n = 2016$ (40% training out of 71^2 samples) with and without weight decay. *Top*: $\eta = 0.0002$ and grokking happens. *Bottom*: $\eta = 0$ and no grokking happens. Weight decay leads to larger $|G_F|$ around epoch 100 and induces grokking behavior. The weights difference ΔW between consecutive weights at time t and $t + 1$, measured by cosine distance, shows two-stage behaviors: first there is huge update on the output weight V , then large update on the hidden weight W . Throughout the training, $\tilde{F}^\top \tilde{F}$ and $P_1^\perp F F^\top$ remains diagonal with up to 8% error, validating our analysis (independent feature learning, Sec. 5). Experiments averaged over 15 seeds.

Feature learning. Previous works treats the NTK as a holistic object and study how it moves away from lazy regime, e.g., it becomes more correlated with task-relevant directions (Kumar et al., 2024; Ba et al., 2022; Damian et al., 2022), becomes adapted to the data (Rubin et al., 2025; Karp et al., 2021), etc. In contrast, our work focuses on explicit learning dynamics of individual features, their interactions, and the transition from memorization to generalization with more samples.

3 PROBLEM FORMULATION

We consider a 2-layer network $\hat{Y} = \sigma(XW)V$ and ℓ_2 loss function on n samples:

$$\min_{V,W} \frac{1}{2} \|P_1^\perp(Y - \hat{Y})\|_F^2 = \min_{V,W} \frac{1}{2} \|P_1^\perp(Y - \sigma(XW)V)\|_F^2 \quad (1)$$

where $P_1^\perp := I - \mathbf{1}\mathbf{1}^\top/n$ is the zero-mean projection matrix along the sample dimension, $Y \in \mathbb{R}^{n \times M}$ is a label matrix (each row is a one-hot vector), $X = [\mathbf{x}_1, \mathbf{x}_2, \dots, \mathbf{x}_n]^\top \in \mathbb{R}^{n \times d}$ is the data matrix, $V \in \mathbb{R}^{K \times M}$ and $W \in \mathbb{R}^{d \times K}$ are the weight matrices of the last layer and hidden layer, respectively. σ is the nonlinear activation function.

In the following, we show that grokking is a consequence of “leaked” backpropagated gradient G_F .

4 STAGE I: LAZY LEARNING (OVERFITTING)

Let $F = \sigma(XW)$ be the activation of the hidden layer and $\tilde{F} = P_1^\perp F$ be the zero-mean version of it. Similarly define $\tilde{Y} = P_1^\perp Y$. We first write down the backpropagated gradient G_F sent to the hidden layer:

$$G_F = -\frac{\partial J}{\partial F} = P_1^\perp(Y - FV)V^\top \quad (2)$$

At the beginning of the training, both W and V are initialized with independent zero-mean random variables. Therefore, the backpropagated gradient G_F is pure random noise. Over time, the hidden activation F is mostly unchanged, and only the output layer learns. In this case, F can be treated as fixed during this stage of learning, and we can prove the following properties of G_F (Sec. C):

Proposition 1. *If \tilde{F} is fixed and is full column rank, entries of $V(0)$ is initialized from normal distribution $N(0, \alpha^2)$ with $0 < \alpha \ll 1$, then $\|G_F(0)\|_F = O(\epsilon\sqrt{KM})$ and the backpropagated gradient G_F is dominated by the term $\tilde{Y}\tilde{Y}^\top F$ at initial time stamps:*

$$G_F(t) = t\tilde{Y}\tilde{Y}^\top \tilde{F} + O(\alpha) + O(\alpha t) + O(t^2) \quad (3)$$

and converges exponentially to the following fixed point when $V = V_{\text{ridge}} = (\tilde{F}^\top \tilde{F} + \eta I)^{-1} \tilde{F}^\top \tilde{Y}$:

$$G_F(+\infty) = \eta(\tilde{F}\tilde{F}^\top + \eta I)^{-1} \tilde{Y}\tilde{Y}^\top \tilde{F}(\tilde{F}^\top \tilde{F} + \eta I)^{-1} \quad (4)$$

162 **G_F at initial phase.** The proposition suggests that for small top layer initialization (measured by
 163 α), $\|G_F\|$ will first increase from $O(\alpha)$ to $O(1)$ and then converge exponentially to $O(\eta)$. Fig. 2
 164 shows that this is indeed the case for $\|G_F\|$, regardless whether grokking happens or not.

165 **G_F at later phase.** The structure of $G_F(+\infty)$ is revealed by the following lemma:

167 **Lemma 1** (Structure of backpropagated gradient G_F). *Assume that (1) entries of W follow standard
 168 normal distribution $N(0, 1)$, (2) $\|\mathbf{x}_i\|_2 = \text{const}$, (3) $\|\mathbf{x}_i^\top \mathbf{x}_{i'} - \rho\|_2 \leq \epsilon$ for all $i \neq i'$ and (4) large
 169 width K , then both $\tilde{F}^\top \tilde{F}$ and $\tilde{F} \tilde{F}^\top$ becomes a multiple of identity and Eqn. 4 becomes:*

$$170 \quad 171 \quad G_F(+\infty) = \frac{\eta}{(Kc_1 + \eta)(nc_2 + \eta)} \tilde{Y} \tilde{Y}^\top \tilde{F} + O(K^{-1}\epsilon) \quad (5)$$

173 where $c_1, c_2 > 0$ are constants related to nonlinearity. When η is small, we have $G_F \propto \eta \tilde{Y} \tilde{Y}^\top \tilde{F}$.
 174 Note that the input features and/or weights can be scaled and what changes is c_1 and c_2 .

175 Interestingly, in both the initial and converging phases, we see that G_F contains a key term $\tilde{Y} \tilde{Y}^\top \tilde{F}$.
 176 As we will see, it plays a critical role in feature learning. From Eqn. 5, it is clear that if $K \rightarrow +\infty$,
 177 then $G_F(+\infty) \rightarrow 0$ and there is no feature learning (i.e., NTK regime). Here we study the case
 178 when K is large (so that Eqn. 5 is valid) but not too large so that feature learning happens.
 179

180 5 STAGE II: INDEPENDENT FEATURE LEARNING

182 5.1 THE ENERGY FUNCTION \mathcal{E}

184 Now let us explore the feature learning process with the help of G_F . Let $W = [\mathbf{w}_1, \mathbf{w}_2, \dots, \mathbf{w}_K]$
 185 where $\mathbf{w}_j \in \mathbb{R}^d$ is the weight vector of j -th node, and $F = [\mathbf{f}_1, \mathbf{f}_2, \dots, \mathbf{f}_K]$ where $\mathbf{f}_j = \sigma(X\mathbf{w}_j) \in$
 186 \mathbb{R}^n is the activation of j -th node. For $G_F \propto \tilde{Y} \tilde{Y}^\top \tilde{F}$, as the structure shown in both initial stage
 187 (Eqn. 3) and later stage (Eqn. 5), the j -th column \mathbf{g}_j of G_F is only dependent on j -th node \mathbf{w}_j , and
 188 thus we can decouple the dynamics into K independent ones, each corresponding to a single node:

$$189 \quad 190 \quad \dot{\mathbf{w}}_j = X^\top D_j \mathbf{g}_j, \quad \mathbf{g}_j \propto \tilde{Y} \tilde{Y}^\top \sigma(X\mathbf{w}_j) \quad (6)$$

191 where $D_j = \text{diag}(\sigma'(X\mathbf{w}_j))$ is the diagonal gating matrix of j -th node. Note that $\tilde{Y}^\top F = \tilde{Y}^\top \tilde{F}$
 192 since P_1^\perp is idempotent. A critical observation here is that Eqn. 6 actually corresponds to the *gradient ascent*
 193 dynamics of the energy function \mathcal{E} .

194 **Theorem 1** (The energy function \mathcal{E} for independent feature learning). *The dynamics (Eqn. 6) of
 195 independent feature learning is exactly the gradient ascent dynamics of the energy function \mathcal{E} w.r.t.
 196 \mathbf{w}_j , a nonlinear canonical-correlation analysis (CCA) between the input X and target \tilde{Y} .*

$$197 \quad 198 \quad \mathcal{E}(\mathbf{w}_j) = \frac{1}{2} \|\tilde{Y}^\top \sigma(X\mathbf{w}_j)\|_2^2 \quad (7)$$

200 Therefore, the feature learned for each node j is the one that maximizes the energy function $\mathcal{E}(\mathbf{w}_j)$.
 201 Since Eqn. 6 can be unbounded, in the following, we put an additional constraint that $\|\mathbf{w}_j\|_2 = 1$
 202 (e.g., because of weight decay). Note that (Tian, 2023) also arrives at an energy function when
 203 studying feature learning in the context of contrastive loss, the resulting function is abstract and
 204 difficult to interpret its structure of its local maxima. Here the structure is much clearer, which we
 205 will explore below.

207 5.2 GROUP ARITHMETIC TASKS

209 To demonstrate a concrete example, we consider *group arithmetic* tasks, i.e., for group H , the task
 210 is to predict $h = h_1 h_2$ given $h_1, h_2 \in H$. One example is the modular addition task $h_1 h_2 = h_1 + h_2$
 211 mod M , which has been extensively studied in grokking (Power et al., 2022; Gromov, 2023; Huang
 212 et al., 2024; Tian, 2025).

213 **The task.** We represent the group elements by one-hot vectors: each data sample $\mathbf{x}_i \in \mathbb{R}^{2M}$ is a
 214 concatenation of two M -dimensional one-hot vectors $(\mathbf{e}_{h_1[i]}, \mathbf{e}_{h_2[i]})$ where $h_1[i]$ and $h_2[i]$ are the
 215 indices of the two one-hot vectors. The output is also a one-hot vector $\mathbf{y}_i = \mathbf{e}_{h_1[i]h_2[i]}$, where
 $1 \leq i \leq n = M^2$. Here the class number $M = |H|$ is the size of the group.

A crash course of group representation theory. A mapping $\rho(h) : H \mapsto \mathbb{C}^{d \times d}$ is called a *group representation* if the group operation is compatible with matrix multiplication: $\rho(h_1)\rho(h_2) = \rho(h_1h_2)$ for any $h_1, h_2 \in H$. Let $R_h \in \mathbb{R}^{M \times M}$ be the *regular representation* of group element h so that $\mathbf{e}_{h_1h_2} = R_{h_1}\mathbf{e}_{h_2}$ for all $h_1, h_2 \in H$, and $P \in \mathbb{R}^{M \times M}$ be the group inverse operator so that $P\mathbf{e}_h = \mathbf{e}_{h^{-1}}$. Note that $P^2 = I$ and $P^\top = P^{-1} = P$.

The decomposition of group representation. The representation theory of finite group (Fulton & Harris, 2013; Steinberg, 2009) says that the regular representation R_h admits a decomposition into complex *irreducible* representations (or *irreps*):

$$R_h = Q \left(\bigoplus_{k=0}^{\kappa(H)} \bigoplus_{r=1}^{m_k} C_k(h) \right) Q^* \quad (8)$$

where $\kappa(H)$ is the number of nontrivial irreps (i.e., not all h map to identity), $C_k(h) \in \mathbb{C}^{d_k \times d_k}$ is the k -th irrep block of R_h , Q is the unitary matrix (and Q^* is its conjugate transpose) and m_k is the multiplicity of the k -th irrep. This means that in the decomposition of R_h , there are m_k copies of d_k -dimensional irrep, and these copies are isomorphic to each other. So the k -th *irrep subspace* \mathcal{H}_k has dimension $m_k d_k$.

For regular representation $\{R_h\}$, one can prove that $m_k = d_k$ for all k and thus $|H| = M = \sum_k d_k^2$. For Abelian group, all complex irreps are 1d (i.e., Fourier bases). One may also choose to do the decomposition in real domain. In this case, a pair of 1d complex irreps will become a 2d real irrep. For example, $e^{i\theta}$ and $e^{-i\theta}$ becomes a 2d matrix $[\cos(\theta), -\sin(\theta); \sin(\theta), \cos(\theta)]$.

5.3 LOCAL MAXIMA OF THE ENERGY FUNCTION

Now we study the local maxima of \mathcal{E} . With the decomposition, we can completely characterize the local maxima of the energy \mathcal{E} with group inputs, even that $\mathcal{E}(\mathbf{w})$ is nonconvex.

Theorem 2 (Local maxima of \mathcal{E} for group input). *For group arithmetics tasks with $\sigma(x) = x^2$, \mathcal{E} has multiple local maxima $\mathbf{w}^* = [\mathbf{u}; \pm P\mathbf{u}]$. Either it is in a real irrep of dimension d_k (with $\mathcal{E}^* = M/8d_k$ and $\mathbf{u} \in \mathcal{H}_k$), or in a pair of complex irrep of dimension d_k (with $\mathcal{E}^* = M/16d_k$ and $\mathbf{u} \in \mathcal{H}_k \oplus \mathcal{H}_{\bar{k}}$). These local maxima are not connected. No other local maxima exist.*

Note that our proof can be extended to more general nonlinearity $\sigma(x) = ax + bx^2$ with $b > 0$ since linear part will be cancelled out due to zero-mean operators. We can show that local maxima of \mathcal{E} are flat, allowing moving around without changing \mathcal{E} :

Corollary 1 (Flatness of local maxima of \mathcal{E} for group input). *Local maxima of \mathcal{E} for group arithmetics tasks with $|H| = M > 2$ are flat, i.e., at least one eigenvalue of its Hessian is zero.*

We can apply the above theorem to the popular modular addition task which is an Abelian group. The resulting representation is Fourier bases.

Corollary 2 (Modular addition). *For modular addition with odd M , all local maxima are single frequency $\mathbf{u}_k = a_k[\cos(km\omega)]_{m=0}^{M-1} + b_k[\sin(km\omega)]_{m=0}^{M-1}$ where $\omega := 2\pi/M$ with $\mathcal{E}^* = M/16$. For even M , $\mathbf{u}_{M/2} \propto [(-1)^m]_{m=0}^{M-1}$ has $\mathcal{E}^* = M/8$. Different local maxima are disconnected.*

Role played by the nonlinearity. With linear activation, there is only one global maximum, which is the maximal eigenvector of $X^\top \tilde{Y} \tilde{Y}^\top X$. This corresponds to Linear Discriminative Analysis (LDA) (Balakrishnama & Ganapathiraju, 1998) that finds directions that maximally separate the class-mean vectors. For group arithmetics tasks, for each target $h = h_1h_2$, each group element (h_1 and h_2) appears once and only once, the class-mean vectors are identical and thus LDA fails to identify any meaningful directions. With nonlinearity, the learned \mathbf{w} has clear meanings.

Meaning of the learned features. First, the learned representation can offer a more efficient reconstruction of the target (see Thm. 3) than simple memorization of all M^2 pairs. Second, learned representations naturally contain useful invariance. For example, some irreps of the cyclic group of \mathbb{Z}_{15} behave like its subgroup \mathbb{Z}_3 and \mathbb{Z}_5 , by mapping its element h to $\text{div}(h, 3)$ and $\text{div}(h, 5)$. If we regard h to be controlled by two hidden factors, then these features lead to focusing on one factor and invariant to others. More importantly, they emerge automatically without explicit supervision.

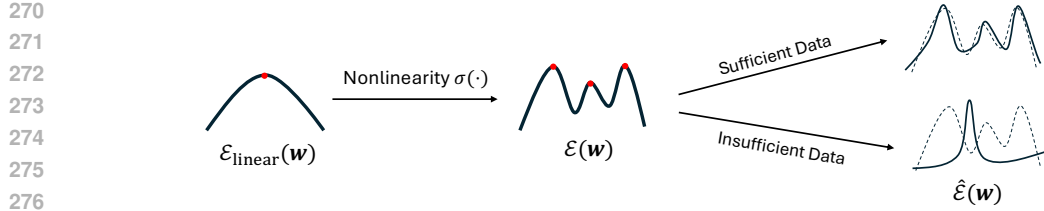


Figure 3: Change of the landscape of the energy function \mathcal{E} (Thm. 1). **Left:** \mathcal{E} with linear activation reduces to simple eigen-decomposition and only have one global maxima. **Middle:** With nonlinearity, the energy landscape now has multiple strict local maxima, each corresponds to a feature (Thm. 2). More importantly, these features are more efficient than memorization in target prediction (Thm. 3). **Right:** With sufficient training data, the landscape remains stable and we can recover these (generalizable) features (Thm. 4), with insufficient data, the landscape changes substantially and local maxima becomes memorization (Thm. 5).

5.4 REPRESENTATION POWER OF LEARNED FEATURES

With Thm. 2, we know that each node of the hidden layers will learn various representations. The question is whether they are sufficient to reconstruct the target \tilde{Y} and how efficient they are.

Theorem 3 (Target Reconstruction). *Assume (1) \mathcal{E} is optimized in complex domain \mathbb{C} , (2) for each irrep k , there are $m_k^2 d_k^2$ pairs of learned weights $\mathbf{w} = [\mathbf{u}; \pm P\mathbf{u}]$ whose associated rank-1 matrices $\{\mathbf{u}\mathbf{u}^*\}$ form a complete bases for \mathcal{H}_k and (3) the top layer V also learns with $\eta = 0$, then $\hat{Y} = \tilde{Y}$.*

From the theorem, we know that $K = 2 \sum_{k \neq 0} m_k^2 d_k^2 \leq 2 [(M - \kappa(H))^2 + \kappa(H) - 1]$ suffice. In particular, for Abelian group, $\kappa(H) = M - 1$ and $K = 2M - 2$. This is much more efficient than pure memorization that requires M^2 nodes, i.e., each node memorizes a single pair $(h_1, h_2) \in H^2$.

Assumptions of the theorem. Assumption (3) is satisfied by training both W and V . Assumption (2) is satisfied since randomly initialized weights typically lead to non-collinear \mathbf{u} . Assumption (1) is necessary due to technical subtleties¹. However, if we change $\mathbf{w} = [\mathbf{u}; \pm P\mathbf{u}]$ slightly to $\mathbf{w} = [\mathbf{u}; \pm P\mathbf{u}']$ in which \mathbf{u}' is a small perturbation of \mathbf{u} , then Thm. 3 holds for real solutions. This happens in the stage III when end-to-end backpropagation refines the representation.

5.5 THE SCALING LAWS OF THE BOUNDARY OF MEMORIZATION AND GENERALIZATION

While Thm. 2 shows the nice structure of local maxima (and features learned), it requires training on all $n = M^2$ pairs of group elements. One may ask whether these representations can still be learned if training on a subset. The answer is yes, by checking the stability of the local maximum.

Theorem 4 (Amount of samples to maintain local optima). *If we select $n \gtrsim d_k^2 M \log(M/\delta)$ data sample from $H \times H$ uniformly at random, then with probability at least $1 - \delta$, the empirical energy function $\hat{\mathcal{E}}$ keeps local maxima for d_k -dimensional irreps (Thm. 2).*

The theorem above states only $O(M \log M)$ samples suffice to learn these features, which will generalize to unseen data according to Thm. 3. Fig. 4 demonstrates that the empirical results closely match the theoretical prediction, and there is a clear phase transition around the boundary (test accuracy $0 \rightarrow 1$), where the training data ratio $p := n/M^2 = O(M^{-1} \log M)$.

Memorization. On the other hand, we can also construct cases when memorization is the only local maximum of \mathcal{E} . This happens when we only collect samples for one target h but missing others, and diversity is in question.

Theorem 5 (Memorization solution). *Let $\phi(x) := \sigma'(x)/x$ and assume $\sigma'(x) > 0$ for $x > 0$. For group arithmetic tasks, suppose we only collect sample $(g, g^{-1}h)$ for one target h with probability p_g . Then the global optimal of \mathcal{E} is a memorization solution, either (1) a focused memorization $\mathbf{w} = \frac{1}{\sqrt{2}}(\mathbf{e}_{g^*}, \mathbf{e}_{g^{-1}h})$ for $g^* = \arg \max p_g$ if ϕ is nondecreasing, or (2) a spreading memorization with $\mathbf{w} = \frac{1}{2} \sum_g s_g [\mathbf{e}_g, \mathbf{e}_{g^{-1}h}]$, if ϕ is strictly decreasing. Here $s_g = \phi^{-1}(2\lambda/p_g)$ and λ is determined by $\sum_g s_g^2 = 2$. No other local optima exist.*

¹The subspace of real orthogonal matrices is not covered by that of symmetric matrices spanned by $\{\mathbf{u}\mathbf{u}^\top\}$. In contrast, the subspace of unitary matrices in complex domain \mathbb{C} can be represented by Hermitian matrices.

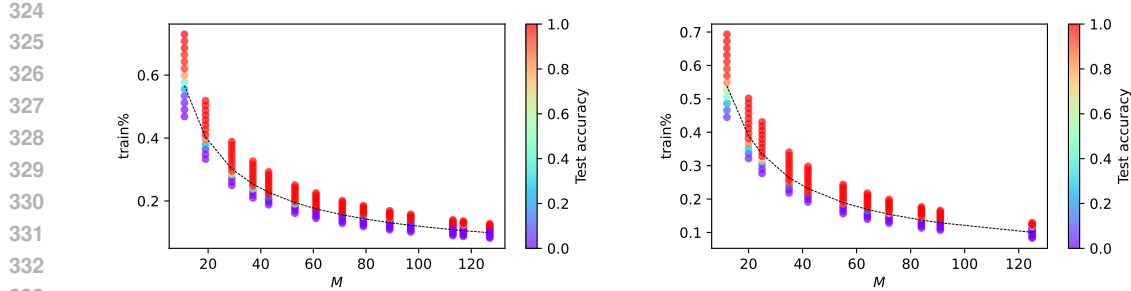


Figure 4: Generalization/memorization phase transition in modular addition tasks. When M grows, the training data ratio $p = n/M^2$ required to achieve generalization decreases. This coincides with Thm. 4 which predicts $p \sim M^{-1} \log M$ (dotted line). We use learning rate 0.0005, weight decay 0.0002 and $K = 2048$. Results averaged over 20 seeds. **Top Left:** Simple cyclic group \mathbb{Z}_M for prime M . **Top Right:** \mathbb{Z}_M for composite M . For more experiments on product and non-Abelian groups, check Fig. 9.

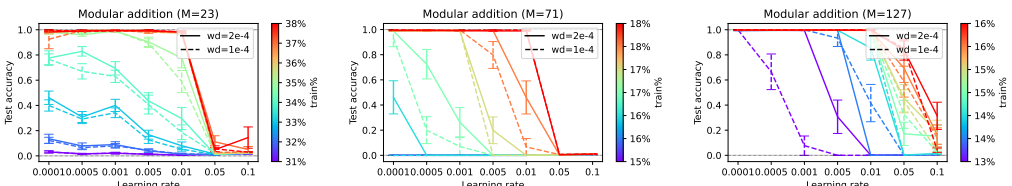


Figure 5: Phase transition from generalizable (gsol) to non-generalizable solutions (ngsol) in modular addition tasks ($M = 23, 71, 127$) with $K = 1024$. Around this critical region, small learning rate more likely lead to gsol, due to the fact that small learning rate keeps the trajectory staying within the basin towards gsol, while large learning rate converges to solutions with higher \mathcal{E} (Fig. 6). Results averaged over 15 seeds.

We can verify that power activations (e.g., $\sigma(x) = x^2$) lead to focused memorization, while more practical ones (e.g., ReLU, SiLU, Tanh and Sigmoid) lead to spreading memorization. We leave it for future work whether this property leads to better results in large scale settings.

Boundary of generalization and memorization (semi-grokked (Varma et al., 2023)). In between the two extreme cases, local maxima of both memorization and generalization may co-exist. In this case, small learning rate keeps the optimization within the attractive basin and converges to gsol, while large learning rate leads to ngsol which has better energy \mathcal{E} (Fig. 6).

Our theory fits well with the empirical observations that there exists a critical data size/ratio (Varma et al., 2023; Wang et al., 2024a; Abramov et al., 2025), above which the grokking suddenly leads to generalization. The observation that memorization energy is higher than generalization (Fig. 6) also explains the *ungrokked/unlearning* phenomenon: a grokked model can move back to memorization when continues to train on a small dataset (Varma et al., 2023; Montanari & Urbani, 2025), and is consistent with (Nguyen & Reddy, 2025) that shows task diversity is important for generalization.

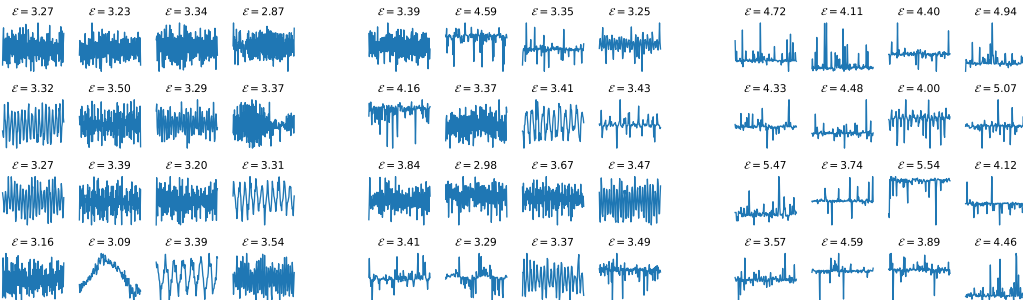


Figure 6: In small data regime of modular addition with $M = 127$ and $n = 3225$ (20% training out of 127^2 samples), Adam optimizer with small learning rate (0.001, left) and (0.002, middle) leads to generalizable solutions (Fourier bases) with low \mathcal{E} , while with large learning rate (0.005, right), Adam found non-generalizable solutions (e.g., memorization) with much higher \mathcal{E} .

378 **6 STAGE III: INTERACTIVE FEATURE LEARNING**
 379

380 The starting point of Stage II is to simplify the exact backpropagated gradient $G_F = P_\eta \tilde{Y} \tilde{Y}^\top \tilde{F} B$
 381 (Eqn. 4) with $B := (\tilde{F}^\top \tilde{F} + \eta I)^{-1}$ to $G_F \propto \eta \tilde{Y} \tilde{Y}^\top F$, by two approximations: (1) $B \propto I$, and (2)
 382 $P_\eta \propto \eta I$. The two approximations are valid due to Thm. 1 when the hidden weights W is randomly
 383 initialized. When training continues, W evolves from random initialization and the conditions may
 384 not hold anymore. In this section we put them back and study their behaviors.

385 **6.1 REPULSION OF SIMILAR FEATURES**
 386

387 We first study the effect of B , which leads to interplay of hidden nodes. Over the training, the
 388 activations of two nodes can be highly correlated and the following theorem shows that similar
 389 features leads to repulsion.

390 **Theorem 6** (Repulsion of similar features). *The j -th column of $\tilde{F} B$ is given by $[\tilde{F} B]_j = b_{jj} \tilde{\mathbf{f}}_j +$
 391 $\sum_{l=1}^K b_{jl} \tilde{\mathbf{f}}_l$, where $\text{sign}(b_{jl}) = -\text{sign}(\tilde{\mathbf{f}}_j^\top P_{\eta, -jl} \tilde{\mathbf{f}}_l)$ and $P_{\eta, -jl} := I - \tilde{F}_{-jl} (\tilde{F}_{-jl}^\top \tilde{F}_{-jl} + \eta I)^{-1} \tilde{F}_{-jl}^\top$
 392 is a projection matrix constructed from \tilde{F}_{-jl} , which is \tilde{F} excluding the l -th and j -th columns.*
 393

394 **Remark.** Intuitively, if $\tilde{\mathbf{f}}_j$ and $\tilde{\mathbf{f}}_l$ are similar, then b_{jl} will be negative and the resulting j and l
 395 columns of $\tilde{F} B$ will be pushed away from each other and vice versa.
 396

397 **6.2 TOP-DOWN MODULATION**
 398

399 Over the training process, it is possible that some local optima are learned first while others learned
 400 later. When the representations are learned partially, the backpropagation offers a mechanism to
 401 focus on missing pieces, by changing the landscape of the energy function \mathcal{E} .

402 **Theorem 7** (Top-down Modulation). *For group arithmetic tasks with $\sigma(x) = x^2$, if the hidden layer
 403 learns only a subset \mathcal{S} of irreps, then the backpropagated gradient $G_F \propto (\Phi_{\mathcal{S}} \otimes \mathbf{1}_M) (\Phi_{\mathcal{S}} \otimes \mathbf{1}_M)^\ast F$
 404 (see proof for the definition of $\Phi_{\mathcal{S}}$), which yields a modified $\mathcal{E}_{\mathcal{S}}$ that only has local maxima on the
 405 missing irreps $k \notin \mathcal{S}$.*

406 **6.3 DIVERSITY ENHANCEMENT WITH MUON**
 407

408 In addition to the mechanism above, certain optimizers (e.g., Muon optimizer (Jordan et al., 2024))
 409 can also address such issue, by boosting the weight update direction that are underrepresented,
 410 enforcing diversity of nodes. While evidence (Tveit et al., 2025) and analysis exist (Shen et al.,
 411 2025) to show that Muon has advantages over other optimizers, to our best knowledge, we are the
 412 first to analyze it in the context of feature learning.

413 Recall that the Muon optimizer converts the gradient $G_W = U_{G_W} D V_{G_W}^\top$ (its SVD decomposition)
 414 to $G'_W = U_{G_W} V_{G_W}^\top$ and update the weight W accordingly (i.e., $\dot{W} \propto G'_W$). We first show that
 415 when Muon is applied to independent feature learning on each \mathbf{w}_j to make them coupled, it still
 416 gives the correct answers to the original optimization problems.

417 **Lemma 2** (Muon optimizes the same as gradient flow). *Muon finds ascending direction to maximize
 418 joint energy $\mathcal{E}_{\text{joint}}(\dot{W}) = \sum_j \mathcal{E}(\mathbf{w}_j)$ and has critical points iff the original gradient G_W vanishes.*
 419

420 Now we show that Muon optimizer can rebalance the gradient updates.

421 **Theorem 8** (Muon rebalances gradient updates). *Consider the following dynamics (Tian, 2023):*

$$\dot{\mathbf{w}} = A(\mathbf{w})\mathbf{w}, \quad \|\mathbf{w}\|_2 \leq 1 \quad (9)$$

422 where $A(\mathbf{w}) := \sum_l \lambda_l(\mathbf{w}) \zeta_l \zeta_l^\top$. Assume that (1) $\{\zeta_l\}$ form orthonormal bases, (2) for $\mathbf{w} =$
 423 $\sum_l \alpha_l \zeta_l$, we have $\lambda_l(\mathbf{w}) = \mu_l \alpha_l$ with $\mu_l \leq 1$, and (3) $\{\alpha_l\}$ is initialized from inverse-exponential
 424 distribution with $\text{CDF}(x) = \exp(-x^{-a})$ with $a > 1$. Then

- 425
- **Independent feature learning.** $\Pr[\mathbf{w} \rightarrow \zeta_l] = p_l := \mu_l^a / \sum_l \mu_l^a$. Then the expected
 426 #nodes to get all local maxima is $T_0 \geq \max\left(1 / \min_l p_l, \sum_{l=1}^L 1/l\right)$.
 - **Muon guiding.** If we use Muon optimizer to optimize K nodes sequentially, then the ex-
 427 pected #nodes to get all local maxima is $T_a = 2^{-a} T_0 + (1 - 2^{-a}) L$. For large a , $T_a \sim L$.

432 The intuition here is that once some weight vectors have “occupied” a local maximum, say ζ_m ,
 433 their gradients point to the same direction (before projecting onto the unit sphere $\|\mathbf{w}\|_2 = 1$), and
 434 the gradient correction of Muon will discount that component from gradients of currently optimized
 435 weight vectors, and keeping them away from ζ_m . In this way, Muon pressed novel gradient direc-
 436 tions and thus encourages exploration. Fig. 7 shows that Muon is effective with limited number of
 437 hidden nodes K .

438 Note that Eqn. 9 is closely related to \mathcal{E} , under the assumption of homogeneous/reversible activation,
 439 i.e., $\sigma(x) = C\sigma'(x)x$ with a constant C (Zhao et al., 2024; Tian et al., 2020). In such setting, Eqn. 6
 440 is related to the gradient dynamics with a PSD matrix $A(\mathbf{w}) = X^\top D(\mathbf{w}) \tilde{Y} \tilde{Y}^\top D(\mathbf{w}) X$.
 441

442 7 EXTENSION TO DEEPER ARCHITECTURES

444 The above analysis and the definition of the energy function \mathcal{E} can be extended to deeper architec-
 445 tures. Consider a multi-layer network with L hidden layers, $F_l = \sigma(F_{l-1}W_l)$ with $F_0 = X$ and
 446 $\hat{Y} = F_L V$. For notation brevity, let $G_l := G_{F_l}$. Let’s see how the gradient backpropagated and how
 447 the learning fits to our framework (Fig. 1).

448 *Stage I.* Stage I does not change since F_L is still a random representation. Then when V starts to
 449 learn and converges, the backpropagated gradient G_L now carries meaningful information: $G_L \propto$
 450 $\tilde{Y} \tilde{Y}^\top F_L$ (Eqn. 5), which initiates Stage II.

451 *Stage II.* We assume homogeneous activation $\sigma(x) = C\sigma'(x)x$. For the next layer $L - 1$, we have:

$$453 \quad G_{L-1} = D_L G_L W_L^\top = D_L (\tilde{Y} \tilde{Y}^\top F_L) W_L^\top = (D_L \tilde{Y} \tilde{Y}^\top D_L) F_{L-1} (W_L W_L^\top) \quad (10)$$

455 since W_L is randomly initialized, we have $W_L W_L^\top \approx I$ and thus $G_{L-1} \propto D_L \tilde{Y} \tilde{Y}^\top D_L F_{L-1}$.

456 Doing this iteratively gives $G_l \propto (\tilde{D}_{l+1} \tilde{Y} \tilde{Y}^\top \tilde{D}_{l+1}) F_l$, where $\tilde{D}_l := \prod_{m=l}^L D_m$. Note that these D
 457 matrices are essentially reweighing/pruning samples randomly, since right now all $\{W_l\}$ are random
 458 except for V . Now the lowest layer receives meaningful backpropagated gradient G_1 that is related
 459 to the target label, and it also exposes to input X . Therefore, the learning starts from there. Once
 460 layer l learns decent representation, layer $l + 1$ receives meaningful input F_l and starts to learn, etc.
 461 When layer l is learning, layer $l' > l$ do not learn since their input $F_{l'}$ remains random noise.
 462

463 From this analysis, we can also see why residual connection helps. In this case, $G_{\text{res},1} = \sum_{l=1}^L G_l$,
 464 in which G_L is definitely a much cleaner and stronger signal, compared to G_1 which undergoes
 465 many random reweighing and pruning of samples.

466 *Stage III.* Once the activation F_l becomes meaningful, top-down modulation could happen (simi-
 467 lar to Thm. 7) among nearby layers so that low-level features can be useful to support high-level
 468 representations. We leave the detailed analysis for future work.
 469

470 8 CONCLUSION, LIMITATIONS AND FUTURE WORK

471 We develop a mathematical framework Li_2 for grokking dynamics in 2-layer networks, identifying
 472 three stages marked by distinct structures of backpropagated gradient G_F . We clarify how various
 473 hyperparameters shape grokking, explain the effectiveness of optimizers like Muon, and extend to
 474 deeper networks. A few interesting implications are listed below. (1) *Two kinds of memorization*.
 475 The “memorization” in grokking is due to overfitting on random features, distinct from memoriza-
 476 tion optima due to limited data (Thm. 5). Grokking switches from overfitting to generalization, not
 477 memorization to generalization. (2) *Flat/sharp optima*. Sharp optima occur when overfitting on
 478 random features (Sec. 4). Local optima from \mathcal{E} are flat (Corollary 1), and over-parameterization
 479 allows multiple nodes to learn similar features, creating flatness. In contrast, Memorization from
 480 limited data requires more nodes, appearing less flat. (3) *Learning rates*. Large learning rates in
 481 Stage I quickly learn V to trigger Stage II. In Stage II, optimal rates depend on data: more data
 482 allows larger rates; limited data needs smaller rates to stay in generalizable basins (Fig. 6).

483 **Limitations.** While the derivation of energy \mathcal{E} is applicable to any input, analysis of its local maxima
 484 relies on restrictive assumption of group structure of the input. Also our analysis does not include
 485 the transition time between consecutive learning stages. We leave them for future work.

486 DISCLOSURE OF LLM USAGE
487488 We have used SoTA LLMs extensively to brainstorm ideas to prove mathematical statements pre-
489 sented in the paper. Specifically, we setup research directions, provide problem setup and intuitions,
490 proposes statements for LLM to analyze and prove, points out key issues in the generated proofs,
491 adjust the statements accordingly and iterate. We also have done extensive experiments to verify
492 the resulting statements. Many proofs proposed by LLMs are incorrect in subtle ways and requires
493 substantial editing and correction. We have carefully revised all the proofs presented in the work,
494 and take full accountability for their correctness.495
496 ETHICS STATEMENT
497498 This work is about investigating various theoretical and empirical properties of neural networks. We
499 do not rely on any sensitive or proprietary data, nor do we use any existing open source models that
500 may produce harmful contents.501
502 REPRODUCIBILITY STATEMENT
503504 All datasets used in this work can be generated synthetically. Models are pretrained from scratch
505 with very small amount of compute. We will release code to support full Reproducibility.506
507 REFERENCES
508

- 509 Roman Abramov, Felix Steinbauer, and Gjergji Kasneci. Grokking in the wild: Data augmentation
510 for real-world multi-hop reasoning with transformers. *arXiv preprint arXiv:2504.20752*, 2025.
- 511 Jimmy Ba, Murat A Erdogdu, Taiji Suzuki, Zhichao Wang, Denny Wu, and Greg Yang. High-
512 dimensional asymptotics of feature learning: How one gradient step improves the representation.
513 *Advances in Neural Information Processing Systems*, 35:37932–37946, 2022.
- 514 Suresh Balakrishnama and Aravind Ganapathiraju. Linear discriminant analysis-a brief tutorial.
515 *Institute for Signal and information Processing*, 18(1998):1–8, 1998.
- 516 Boaz Barak, Benjamin Edelman, Surbhi Goel, Sham Kakade, Eran Malach, and Cyril Zhang. Hidden
517 progress in deep learning: Sgd learns parities near the computational limit. *Advances in
518 Neural Information Processing Systems*, 35:21750–21764, 2022.
- 519 Lenaic Chizat, Edouard Oyallon, and Francis Bach. On lazy training in differentiable programming.
520 *Advances in neural information processing systems*, 32, 2019.
- 521 Tianzhe Chu, Yuexiang Zhai, Jihan Yang, Shengbang Tong, Saining Xie, Dale Schuurmans, Quoc V
522 Le, Sergey Levine, and Yi Ma. Sft memorizes, rl generalizes: A comparative study of foundation
523 model post-training. *arXiv preprint arXiv:2501.17161*, 2025.
- 524 Kenzo Clauw, Sebastiano Stramaglia, and Daniele Marinazzo. Information-theoretic progress mea-
525 sures reveal grokking is an emergent phase transition. *arXiv preprint arXiv:2408.08944*, 2024.
- 526 Alexandru Damian, Jason Lee, and Mahdi Soltanolkotabi. Neural networks can learn representations
527 with gradient descent. In *Conference on Learning Theory*, pp. 5413–5452. PMLR, 2022.
- 528 Clémentine CJ Dominé, Nicolas Anguita, Alexandra M Proca, Lukas Braun, Daniel Kunin, Pe-
529 dro AM Mediano, and Andrew M Saxe. From lazy to rich: Exact learning dynamics in deep
530 linear networks. *arXiv preprint arXiv:2409.14623*, 2024.
- 531 Darshil Doshi, Aritra Das, Tianyu He, and Andrey Gromov. To grok or not to grok: Disen-
532 tangling generalization and memorization on corrupted algorithmic datasets. *arXiv preprint
533 arXiv:2310.13061*, 2023.
- 534 Darshil Doshi, Tianyu He, Aritra Das, and Andrey Gromov. Grokking modular polynomials. *arXiv
535 preprint arXiv:2406.03495*, 2024.

- 540 Philippe Flajolet, Daniele Gardy, and Loÿs Thimonier. Birthday paradox, coupon collectors, caching
 541 algorithms and self-organizing search. *Discrete Applied Mathematics*, 39(3):207–229, 1992.
 542
- 543 William Fulton and Joe Harris. *Representation theory: a first course*, volume 129. Springer Science
 544 & Business Media, 2013.
- 545 Andrey Gromov. Grokking modular arithmetic. *arXiv preprint arXiv:2301.02679*, 2023.
 546
- 547 Yufei Huang, Shengding Hu, Xu Han, Zhiyuan Liu, and Maosong Sun. Unified view of grokking,
 548 double descent and emergent abilities: A perspective from circuits competition. *arXiv preprint*
 549 *arXiv:2402.15175*, 2024.
- 550 Keller Jordan, Yuchen Jin, Vlado Boza, Jiacheng You, Franz Cesista, Laker Newhouse, and Jeremy
 551 Bernstein. Muon: An optimizer for hidden layers in neural networks. 2024. URL <https://kellerjordan.github.io/posts/muon/>.
 552
- 553 Stefani Karp, Ezra Winston, Yuanzhi Li, and Aarti Singh. Local signal adaptivity: Provable feature
 554 learning in neural networks beyond kernels. *Advances in Neural Information Processing Systems*,
 555 34:24883–24897, 2021.
- 556 Tanishq Kumar, Blake Bordelon, Samuel J. Gershman, and Cengiz Pehlevan. Grokking as the transi-
 557 tion from lazy to rich training dynamics, 2024. URL <https://arxiv.org/abs/2310.06110>.
 558
- 559 Aitor Lewkowycz and Guy Gur-Ari. On the training dynamics of deep networks with l_2 regular-
 560 ization. *Advances in Neural Information Processing Systems*, 33:4790–4799, 2020.
- 561 Ziming Liu, Ouail Kitouni, Niklas S Nolte, Eric Michaud, Max Tegmark, and Mike Williams. To-
 562 wards understanding grokking: An effective theory of representation learning. *Advances in Neu-
 563 ral Information Processing Systems*, 35:34651–34663, 2022.
- 564 Ziming Liu, Eric J Michaud, and Max Tegmark. Omnidrok: Grokking beyond algorithmic data.
 565 In *The Eleventh International Conference on Learning Representations*, 2023. URL <https://openreview.net/forum?id=zDiHoIWa0q1>.
 566
- 567 William Merrill, Nikolaos Tsilivis, and Aman Shukla. A tale of two circuits: Grokking as competi-
 568 tion of sparse and dense subnetworks. *arXiv preprint arXiv:2303.11873*, 2023.
- 569 Beren Millidge. Grokking 'grokking', 2022. URL <https://www.beren.io/2022-01-11-Grokking-Grokking/>.
 570
- 571 Iman Mirzadeh, Keivan Alizadeh, Hooman Shahrokhi, Oncel Tuzel, Samy Bengio, and Mehrdad
 572 Farajtabar. Gsm-symbolic: Understanding the limitations of mathematical reasoning in large
 573 language models. *arXiv preprint arXiv:2410.05229*, 2024.
- 574 Mohamad Amin Mohamadi, Zhiyuan Li, Lei Wu, and Danica J Sutherland. Why do you grok? a
 575 theoretical analysis of grokking modular addition. *arXiv preprint arXiv:2407.12332*, 2024.
- 576 Andrea Montanari and Gabriele Urbani. Dynamical decoupling of generalization and overfitting in
 577 large two-layer networks, 2025.
- 578 Depen Morwani, Benjamin L Edelman, Costin-Andrei Oncescu, Rosie Zhao, and Sham Kakade.
 579 Feature emergence via margin maximization: case studies in algebraic tasks. *arXiv preprint*
 580 *arXiv:2311.07568*, 2023.
- 581 Neel Nanda, Lawrence Chan, Tom Lieberum, Jess Smith, and Jacob Steinhardt. Progress measures
 582 for grokking via mechanistic interpretability. In *The Eleventh International Conference on Learn-
 583 ing Representations*, 2023. URL <https://openreview.net/forum?id=9XF8DPmdW>.
 584
- 585 Alex Nguyen and Gautam Reddy. Differential learning kinetics govern the transition from mem-
 586 orization to generalization during in-context learning. In *The Thirteenth International Confer-
 587 ence on Learning Representations*, 2025. URL <https://openreview.net/forum?id=INy17qUdjZ>.
 588

- 594 Alethea Power, Yuri Burda, Harri Edwards, Igor Babuschkin, and Vedant Misra. Grokking: Gen-
 595 eralization beyond overfitting on small algorithmic datasets. *arXiv preprint arXiv:2201.02177*,
 596 2022.
- 597 Lucas Prieto, Melih Barsbey, Pedro AM Mediano, and Tolga Birdal. Grokking at the edge of nu-
 598 matical stability. *arXiv preprint arXiv:2501.04697*, 2025.
- 600 Noa Rubin, Inbar Seroussi, and Zohar Ringel. Grokking as a first order phase transition in two layer
 601 networks. *ICLR*, 2024.
- 602 Noa Rubin, Kirsten Fischer, Javed Lindner, David Dahmen, Inbar Seroussi, Zohar Ringel, Michael
 603 Krämer, and Moritz Helias. From kernels to features: A multi-scale adaptive theory of feature
 604 learning. *arXiv preprint arXiv:2502.03210*, 2025.
- 606 Wei Shen, Ruichuan Huang, Minhui Huang, Cong Shen, and Jiawei Zhang. On the convergence
 607 analysis of muon. *arXiv preprint arXiv:2505.23737*, 2025.
- 608 Maor Shutman, Oren Louidor, and Ran Tessler. Learning words in groups: fusion algebras, tensor
 609 ranks and grokking. *arXiv preprint arXiv:2509.06931*, 2025.
- 611 Benjamin Steinberg. Representation theory of finite groups. *Carleton University*, 2009.
- 612 Vimal Thilak, Eta Littwin, Shuangfei Zhai, Omid Saremi, Roni Paiss, and Joshua Susskind. The
 613 slingshot mechanism: An empirical study of adaptive optimizers and the grokking phenomenon.
 614 *arXiv preprint arXiv:2206.04817*, 2022.
- 616 Yuandong Tian. Understanding the role of nonlinearity in training dynamics of contrastive learning.
 617 In *The Eleventh International Conference on Learning Representations*, 2023. URL https://openreview.net/forum?id=s130rTE3U_X.
- 619 Yuandong Tian. Composing global solutions to reasoning tasks via algebraic objects in neural nets.
 620 *NeurIPS*, 2025.
- 622 Yuandong Tian, Lantao Yu, Xinlei Chen, and Surya Ganguli. Understanding self-supervised learning
 623 with dual deep networks. *arXiv preprint arXiv:2010.00578*, 2020.
- 624 Joel A Tropp. User-friendly tail bounds for sums of random matrices. *Foundations of computational
 625 mathematics*, 12(4):389–434, 2012.
- 627 Amund Tveit, Bjørn Remseth, and Arve Skogvold. Muon optimizer accelerates grokking. *arXiv
 628 preprint arXiv:2504.16041*, 2025.
- 629 Vikrant Varma, Rohin Shah, Zachary Kenton, János Kramár, and Ramana Kumar. Explaining
 630 grokking through circuit efficiency. *arXiv preprint arXiv:2309.02390*, 2023.
- 632 Boshi Wang, Xiang Yue, Yu Su, and Huan Sun. Grokked transformers are implicit reasoners: A
 633 mechanistic journey to the edge of generalization. *arXiv preprint arXiv:2405.15071*, 2024a.
- 634 Xinyi Wang, Antonis Antoniades, Yanai Elazar, Alfonso Amayuelas, Alon Albalak, Kexun Zhang,
 635 and William Yang Wang. Generalization vs memorization: Tracing language models’ capabilities
 636 back to pretraining data. *arXiv preprint arXiv:2407.14985*, 2024b.
- 638 Zhiwei Xu, Yutong Wang, Spencer Frei, Gal Vardi, and Wei Hu. Benign overfitting and grokking in
 639 relu networks for xor cluster data. *arXiv preprint arXiv:2310.02541*, 2023.
- 640 Jiawei Zhao, Zhenyu Zhang, Beidi Chen, Zhangyang Wang, Anima Anandkumar, and Yuandong
 641 Tian. Galore: Memory-efficient llm training by gradient low-rank projection. *ICML*, 2024.
- 642
- 643
- 644
- 645
- 646
- 647

648 A INDEPENDENT FEATURE LEARNING (SEC. 5)
649650 **Lemma 3.** Let $\phi_n(z) := \text{He}_n(z)/\sqrt{n!}$ be the orthonormal Hermite system on $L^2(\gamma)$. If (Z_1, Z_2)
651 are standard normals with correlation ρ , then
652

653
$$\mathbb{E}[\phi_n(Z_1) \phi_m(Z_2)] = \rho^n \delta_{nm} \quad (n, m \geq 0).$$

654

655 *Proof of Lemma 3.* Use the generating function² $\exp(tz - \frac{t^2}{2}) = \sum_{k \geq 0} \phi_k(z) t^k$ for $z \sim \mathcal{N}(0, 1)$.
656 Then, for correlated normals (Z_1, Z_2) with correlation ρ ,

657
$$\mathbb{E}\left[e^{tZ_1 - \frac{t^2}{2}} e^{uZ_2 - \frac{u^2}{2}}\right] = \exp(\rho tu) = \sum_{k \geq 0} \rho^k (tu)^k.$$

658
659

660 Expanding the left-hand side by the generating functions and matching coefficients of $t^n u^m$ yields
661 $\mathbb{E}[\phi_n(Z_1) \phi_m(Z_2)] = \rho^n \delta_{nm}$.
662663 To show why $\mathbb{E}\left[e^{tZ_1 - \frac{t^2}{2}} e^{uZ_2 - \frac{u^2}{2}}\right] = \exp(\rho tu)$ is correct, decompose (Z_1, Z_2) into Gaussian
664 independent random variables (X, Y) :

665
$$Z_1 := X, \quad Z_2 := \rho X + \sqrt{1 - \rho^2} Y,$$

666

667 Then we have

668
$$\begin{aligned} \mathbb{E}\left[e^{tZ_1 - \frac{t^2}{2}} e^{uZ_2 - \frac{u^2}{2}}\right] &= \mathbb{E}\left[e^{tX - \frac{t^2}{2}} e^{u(\rho X + \sqrt{1 - \rho^2} Y) - \frac{u^2}{2}}\right] \\ 669 &= \mathbb{E}\left[e^{(t + \rho u)X - \frac{t^2}{2}}\right] \mathbb{E}\left[e^{u\sqrt{1 - \rho^2} Y - \frac{u^2}{2}}\right]. \end{aligned}$$

670
671

672 For $G \sim \mathcal{N}(0, 1)$ we have $\mathbb{E}[e^{aG}] = e^{a^2/2}$, hence $\mathbb{E}\left[e^{aG - \frac{a^2}{2}}\right] = 1$ due to Lemma 4. Applying this
673 twice,
674

675
$$\begin{aligned} \mathbb{E}\left[e^{(t + \rho u)X - \frac{t^2}{2}}\right] &= \exp\left(\frac{(t + \rho u)^2}{2} - \frac{t^2}{2}\right) = \exp\left(\rho tu + \frac{\rho^2 u^2}{2}\right), \\ 676 \mathbb{E}\left[e^{u\sqrt{1 - \rho^2} Y - \frac{u^2}{2}}\right] &= \exp\left(\frac{u^2(1 - \rho^2)}{2} - \frac{u^2}{2}\right) = \exp\left(-\frac{\rho^2 u^2}{2}\right). \end{aligned}$$

677
678

679 Multiplying the two factors yields
680

681
$$\exp\left(\rho tu + \frac{\rho^2 u^2}{2}\right) \exp\left(-\frac{\rho^2 u^2}{2}\right) = \exp(\rho tu),$$

682

683 as claimed. □
684685 **Lemma 4** (Moment identity). For $X \sim \mathcal{N}(0, 1)$, $\mathbb{E}[e^{tX}] = \exp(t^2/2)$. Equivalently, $\mathbb{E}[e^{tX - t^2/2}] = 1$.
686687 *Proof.* Complete the square:
688

689
$$\mathbb{E}[e^{tX}] = \frac{1}{\sqrt{2\pi}} \int_{\mathbb{R}} e^{tx} e^{-x^2/2} dx = \frac{1}{\sqrt{2\pi}} \int e^{-(x-t)^2/2} e^{t^2/2} dx = \exp\left(\frac{t^2}{2}\right).$$

690

691 □692 **Lemma 1** (Structure of backpropagated gradient G_F). Assume that (1) entries of W follow standard
693 normal distribution $N(0, 1)$, (2) $\|\mathbf{x}_i\|_2 = \text{const}$, (3) $\|\mathbf{x}_i^\top \mathbf{x}_{i'} - \rho\|_2 \leq \epsilon$ for all $i \neq i'$ and (4) large
694 width K , then both $\tilde{F}^\top \tilde{F}$ and $\tilde{F} \tilde{F}^\top$ becomes a multiple of identity and Eqn. 4 becomes:
695

696
$$G_F(+\infty) = \frac{\eta}{(Kc_1 + \eta)(nc_2 + \eta)} \tilde{Y} \tilde{Y}^\top \tilde{F} + O(K^{-1}\epsilon) \quad (5)$$

697

698 where $c_1, c_2 > 0$ are constants related to nonlinearity. When η is small, we have $G_F \propto \eta \tilde{Y} \tilde{Y}^\top \tilde{F}$.
699 Note that the input features and/or weights can be scaled and what changes is c_1 and c_2 .
700701

 ²https://en.wikipedia.org/wiki/Hermite_polynomials

702 *Proof.* In the following, we will prove that (1) $\tilde{F}^\top \tilde{F}$ is a multiple of identity and (2) $FF^\top \propto \alpha I + \beta \mathbf{1}\mathbf{1}^\top$. Without loss of generality, we assume that entry of W follows standard normal distribution $\mathcal{N}(0, 1)$.

703 **$\tilde{F}^\top \tilde{F}$ is a multiple of identity.** Since each column of \tilde{F} is $P_1^\perp \sigma(X \mathbf{w}_j)$ a zero-mean n -dimensional
704 random vector and columns are i.i.d. due to the independence of columns of W . With large width
705 K , $\tilde{F}^\top \tilde{F}$ becomes a multiple of identity.

706 **FF^\top is a diagonal plus an all-constant matrix.** Note that the i -th row of F is
707 $[\sigma(\mathbf{w}_1^\top \mathbf{x}_i), \sigma(\mathbf{w}_2^\top \mathbf{x}_i), \dots, \sigma(\mathbf{w}_K^\top \mathbf{x}_i)]$, with large width K , the inner product between the i -th row
708 and j -th row of F approximates to $K\mathcal{K}(i, j)$ where $\mathcal{K}(i, j)$ is defined as follows:

$$709 \quad \mathcal{K}(i, j) = \mathbb{E}_{\mathbf{w}}[\sigma(\mathbf{w}^\top \mathbf{x}_i)\sigma(\mathbf{w}^\top \mathbf{x}_j)] \quad (11)$$

710 To estimate the entry $\mathcal{K}(i, j)$, we first do standardization by setting $Z_1 := \mathbf{w}^\top \mathbf{x}_i / s_i$ and $Z_2 :=$
711 $\mathbf{w}^\top \mathbf{x}_j / s_j$ where $s_i = \|\mathbf{x}_i\|_2$ and $s_j = \|\mathbf{x}_j\|_2$. Then (Z_1, Z_2) are standard normals with
712 $\text{Corr}(Z_1, Z_2) = \rho_{ij}$, and $\mathcal{K}(i, j) = \mathbb{E}[\sigma(s_i Z_1)\sigma(s_j Z_2)]$.

713 Let $\phi_l(z) := \text{He}_l(z)/\sqrt{l!}$ be the orthonormal Hermite system on $L^2(\gamma)$, where γ is the standard
714 Gaussian measure and He_l are the Hermite polynomials. For $s \geq 0$ define $f_s(z) := \sigma(sz)$. By the
715 $L^2(\gamma)$ assumption, $f_s = \sum_{n=0}^{\infty} a_l(s) \phi_l$ with

$$716 \quad a_l(s) = \langle f_s, \phi_l \rangle_{L^2(\gamma)} = \frac{1}{\sqrt{l!}} \mathbb{E}[\sigma(sZ) \text{He}_l(Z)].$$

717 Thus

$$718 \quad \sigma(s_i Z_1) = \sum_{l \geq 0} a_l(s_i) \phi_l(Z_1), \quad \sigma(s_j Z_2) = \sum_{l \geq 0} a_l(s_j) \phi_l(Z_2).$$

719 By bilinearity and Lemma 3,

$$720 \quad \begin{aligned} \mathcal{K}(i, j) &= \mathbb{E} \left[\sum_{l \geq 0} a_l(s_i) \phi_l(Z_1) \sum_{m \geq 0} a_m(s_j) \phi_m(Z_2) \right] = \sum_{l, m \geq 0} a_l(s_i) a_m(s_j) \mathbb{E}[\phi_l(Z_1) \phi_m(Z_2)] \\ 721 &= \sum_{l \geq 0} a_l(s_i) a_l(s_j) \rho_{ij}^l. \end{aligned}$$

722 If $s_i \equiv 1$ and $\|\rho_{ij} - \rho\|_2 \leq \epsilon$ for $i \neq j$, then

$$723 \quad \mathcal{K}(i, i) = \sum_{l \geq 0} a_l^2(s) =: a$$

724 Let $c := \sum_{l \geq 1} l a_l^2(s) < +\infty$ (it is convergent due to the big factor $l!$ in the denominator). Let
725 $b := \sum_{l \geq 0} a_l^2(s) \rho^l$ and we have for all $i \neq j$:

$$726 \quad \|\mathcal{K}(i, j) - b\|_2 \leq \sum_{l \geq 0} a_l^2(s) \|\rho_{ij}^l - \rho^l\|_2 \leq \sum_{l \geq 1} l a_l^2(s) \epsilon = c\epsilon$$

727 due to the fact that $\|\rho_{ij}^l - \rho^l\|_2 \leq l \xi^{l-1} \epsilon$ for all $l \geq 1$ and some ξ in between ρ_{ij} and ρ . hence
728 $\mathcal{K}(i, j) = (a - b)\delta_{ij} + b + O(\epsilon)$ and thus $FF^\top = K(a - b)I + Kb\mathbf{1}\mathbf{1}^\top + O(K\epsilon)\mathbf{1}\mathbf{1}^\top$. Note that
729 by Parseval's identity, $a = \mathbb{E}_{Z \sim \mathcal{N}(0, 1)}[\sigma^2(sZ)]$.

730 Therefore, $\tilde{F}\tilde{F}^\top = K(a - b + O(\epsilon))P_1^\perp = K(a - b + O(\epsilon))(I - \mathbf{1}\mathbf{1}^\top/n) + O(K\epsilon)\mathbf{1}\mathbf{1}^\top$ and $P_\eta \tilde{Y} =$
731 $\frac{\eta}{K(a-b)+\eta} \tilde{Y}$. Since $\tilde{F}^\top \tilde{F}$ is proportional to identity matrix, $(\tilde{F}^\top \tilde{F} + \eta I)^{-1}$ is also proportional to
732 identity matrix and the conclusion follows. \square

733 A.1 THE ENERGY FUNCTION \mathcal{E} (SEC. 5.3)

734 **Theorem 1** (The energy function \mathcal{E} for independent feature learning). *The dynamics (Eqn. 6) of
735 independent feature learning is exactly the gradient ascent dynamics of the energy function \mathcal{E} w.r.t.
736 \mathbf{w}_j , a nonlinear canonical-correlation analysis (CCA) between the input X and target \tilde{Y} .*

$$737 \quad \mathcal{E}(\mathbf{w}_j) = \frac{1}{2} \|\tilde{Y}^\top \sigma(X \mathbf{w}_j)\|_2^2 \quad (7)$$

756 *Proof.* Taking gradient of \mathcal{E} w.r.t. \mathbf{w}_j , and we have $\cdot \mathbf{w}_j = X^\top D_j \tilde{Y} \tilde{Y}^\top \sigma(X \mathbf{w}_j)$, which proves the
 757 theorem. \square

758
 759 **Theorem 2** (Local maxima of \mathcal{E} for group input). *For group arithmetics tasks with $\sigma(x) = x^2$,
 760 \mathcal{E} has multiple local maxima $\mathbf{w}^* = [\mathbf{u}; \pm P\mathbf{u}]$. Either it is in a real irrep of dimension d_k (with
 761 $\mathcal{E}^* = M/8d_k$ and $\mathbf{u} \in \mathcal{H}_k$), or in a pair of complex irrep of dimension d_k (with $\mathcal{E}^* = M/16d_k$ and
 762 $\mathbf{u} \in \mathcal{H}_k \oplus \mathcal{H}_{\bar{k}}$). These local maxima are not connected. No other local maxima exist.*

763
 764 *Proof.* Following this setting, if ordered by target values, we can write down the data matrix
 765 $X = [X_{h_1}; X_{h_2}; \dots; X_{h_M}]$ (i.e., each X_h occupies M rows of X) in which each $X_h = [R_h^\top, P] \in$
 766 $\mathbb{R}^{M \times 2M}$. Here R_h is the *regular representation* (a special case of permutation representation) of
 767 group element h so that $\mathbf{e}_{h_1 h_2} = R_{h_1} \mathbf{e}_{h_2}$ for all $h_1, h_2 \in H$, and P is the group inverse operator so
 768 that $P\mathbf{e}_h = \mathbf{e}_{h^{-1}}$. This is because each row of X that corresponds to the target h can be written as
 769 $[\mathbf{e}_{h_1 h_2}^\top, \mathbf{e}_{h_1^{-1}}^\top] = [\mathbf{e}_{h_1}^\top R_h^\top, \mathbf{e}_{h_1}^\top P]$. Stacking the rows that lead to target h together, and order them by
 770 h_1 , we get $X_h = [R_h^\top, P]$.

771 Let $\mathbf{w} = [\mathbf{u}; Pv]$. Let matrix $S_{ij} := \sigma(u_i + v_j)$, since R_h is a permutation matrix, then $\sigma(X_h \mathbf{w}) =$
 772 $\sigma(R_h^\top \mathbf{u} + \mathbf{v})$ is a row shuffling of S . Therefore, $\sigma(X_h \mathbf{w}) = \text{diag}(R_h^\top S) \mathbf{1}_M$, where $\text{diag}(\cdot)$ is the
 773 diagonal of a matrix. Note that in this target label ordering, we have $Y = I_M \otimes \mathbf{1}_M$. So for each
 774 column h of Y , we have $\mathbf{y}_h = \mathbf{e}_h \otimes \mathbf{1}_M$. So

$$775 \quad z_h := \mathbf{y}_h^\top \sigma(X \mathbf{w}) = \mathbf{1}_M^\top \sigma(X_h \mathbf{w}) = \mathbf{1}_M^\top \text{diag}(R_h^\top S) \mathbf{1}_M = \text{tr}(R_h^\top S) = \langle R_h, S \rangle_F \quad (12)$$

776 where $\langle A, B \rangle_F := \text{tr}(A^\top B)$ is the Frobenius inner product. And the energy \mathcal{E} can be written as:

$$777 \quad \mathcal{E}(\mathbf{w}) = \frac{1}{2} \sum_h (z_h - \bar{z})^2 \quad (13)$$

781 where $\bar{z} := \frac{1}{M} \sum_h z_h = \frac{1}{M} \sum_h \langle R_h, S \rangle_F = \langle \frac{1}{M} \sum_h R_h, S \rangle_F = \frac{1}{M} \langle \mathbf{1}_M \mathbf{1}_M^\top, S \rangle_F$. Therefore,
 782 using $R_h \mathbf{1}_M = \mathbf{1}_M$, $\mathcal{E}(\mathbf{w})$ can be written as:

$$783 \quad \mathcal{E}(\mathbf{w}) = \frac{1}{2} \sum_h \langle \tilde{R}_h, S \rangle_F^2 \quad (14)$$

786 where $\tilde{R}_h = R_h P_1^\perp$. Now we study its property. We decompose $\{\tilde{R}_h\}$ into complex irreducible
 787 representations:

$$788 \quad \tilde{R}_h = Q \left(\bigoplus_{k \neq 0} \bigoplus_{r=1}^{m_k} C_k(h) \right) Q^* \quad (15)$$

789 where $C_k(h)$ is the k -th irreducible representation block of R_h , Q is the unitary matrix (and Q^* is
 790 the conjugate transpose of Q) and m_k is the multiplicity of the k -th irreducible representation. Since
 791 \tilde{R}_h is a zero-meaned representation, we remove the trivial representation $C_0(h)$ and thus $Q^* \mathbf{1} = 0$.
 792 Let $\hat{S} = Q^\top S Q$. Then

$$793 \quad \langle \tilde{R}_h, S \rangle_F = \langle Q \left(\bigoplus_{k \neq 0} \bigoplus_{r=1}^{m_k} C_k(h) \right) Q^*, S \rangle_F = \langle \bigoplus_{k \neq 0} \bigoplus_{r=1}^{m_k} C_k(h), \hat{S} \rangle_F = \sum_{k \neq 0} \sum_{r=1}^{m_k} \text{tr}(C_k^*(h) \hat{S}_{k,r}) \quad (16)$$

794 where $\hat{S}_{k,r}$ is the (k, r) -th principle (diagonal) block of \hat{S} . Therefore, we have:

$$801 \quad \sum_h \langle \tilde{R}_h, S \rangle_F^2 = \sum_h \sum_{(k,r),(k',r')} \text{tr}(C_k^*(h) \hat{S}_{k,r}) \text{tr}(C_{k'}^*(h) \hat{S}_{k',r'}) \quad (17)$$

$$804 \quad = \sum_{(k,r),(k',r')} \text{vec}^*(\hat{S}_{k,r}) \left[\sum_h \text{vec}(C_k(h)) \text{vec}(C_{k'}^*(h)) \right] \text{vec}(\hat{S}_{k',r'}) \quad (18)$$

808 **Case 1.** If $k \neq k'$ are inequivalent irreducible representations of dimension d_k and $d_{k'}$, then we can
 809 prove that $\sum_h \text{vec}(C_k(h)) \text{vec}(C_{k'}^*(h)) = 0$. To see this, let $\mathbf{A}_{k,k'}(Z) = \sum_h C_k(h) Z C_{k'}^{-1}(h)$, then
 $\mathbf{A}_{k,k'}(Z)$ is a H -invariant linear mapping from d_k to $d_{k'}$ dimensional space. Thus by Schur's lemma,

810 $\mathbf{A}_{k,k'}(Z) = 0$ for any Z . But since $\text{vec}(\mathbf{A}_{k,k'}(Z)) = (\sum_h \bar{C}_{k'}(h) \otimes C_k(h)) \text{vec}(Z)$, we have
 811 $\sum_h \bar{C}_{k'}(h) \otimes C_k(h) = 0$. Expanding each component, we have $\sum_h \text{vec}(C_k(h)) \text{vec}(C_{k'}^*(h)) = 0$.
 812

813 **Case 2.** If $k = k'$ are equivalent irreducible representations (and both have dimension d_k), then we
 814 can prove that $\sum_h \text{vec}(C_k(h)) \text{vec}(C_k^*(h)) = \frac{M}{d_k} \text{vec}(I_{d_k}) \text{vec}^*(I_{d_k})$. Then with Schur's average
 815 lemma, we have $\mathbf{A}_{kk}(Z) = \frac{M}{d_k} \text{tr}(Z) I_{d_k}$. A vectorization leads to $(\sum_h \bar{C}_k(h) \otimes C_k(h)) \text{vec}(Z) =$
 816 $\frac{M}{d_k} \text{tr}(Z) \text{vec}(I_{d_k})$. Notice that $\text{vec}^*(I_{d_k}) \text{vec}(Z) = \text{tr}(Z)$ and we arrive at the conclusion.
 817

818 Therefore, for the objective function we have:

$$819 \mathcal{E}(\mathbf{w}) = \frac{1}{2} \sum_h \langle \tilde{R}_h, S \rangle_F^2 = \frac{M}{2} \sum_{k \neq 0} \frac{1}{d_k} \left| \sum_r \text{tr}(\hat{S}_{k,r}) \right|^2 \quad (19)$$

822 **Special case of quadratic activation.** If $\sigma(x) = x^2$, then we have $S = (\mathbf{u} \circ \mathbf{u}) \mathbf{1}^\top + \mathbf{1}(\mathbf{v} \circ \mathbf{v}) + \mathbf{u}\mathbf{v}^\top$
 823 and thus $\hat{S} = \hat{\mathbf{u}}\hat{\mathbf{v}}^*$, where $\hat{\mathbf{u}} = Q^*\mathbf{u}$ and $\hat{\mathbf{v}} = Q^*\mathbf{v}$. Therefore, since $Q^*\mathbf{1} = 0$, $\hat{S}_{k,r} = \hat{\mathbf{u}}_{k,r}\hat{\mathbf{v}}_{k,r}^*$ and
 824 $\text{tr}(\hat{S}_{k,r}) = \hat{\mathbf{u}}_{k,r}^*\hat{\mathbf{v}}_{k,r}$. Therefore, with Cauchy-Schwarz inequality, we have
 825

$$826 \mathcal{E} = \frac{1}{2} \sum_h \langle \tilde{R}_h, S \rangle_F^2 = \frac{M}{2} \sum_{k \neq 0} \frac{1}{d_k} \left| \sum_r \hat{\mathbf{u}}_{k,r}^* \hat{\mathbf{v}}_{k,r} \right|^2 \leq \frac{M}{2} \sum_{k \neq 0} \frac{1}{d_k} \left(\sum_r |\hat{\mathbf{u}}_{k,r}|^2 \right) \left(\sum_r |\hat{\mathbf{v}}_{k,r}|^2 \right) \quad (20)$$

830 Let $a_k = \sum_r |\hat{\mathbf{u}}_{k,r}|^2$, $b_k = \sum_r |\hat{\mathbf{v}}_{k,r}|^2$, and $c_k = a_k + b_k \geq 0$. Then we have:

$$831 \mathcal{E} = \frac{1}{2} \sum_h \langle \tilde{R}_h, S \rangle_F^2 \leq \frac{M}{2} \sum_{k \neq 0} \frac{a_k b_k}{d_k} \leq \frac{M}{8} \sum_{k \neq 0} \frac{c_k^2}{d_k}, \quad \text{subject to } \sum_{k \neq 0} c_k = 1 \quad (21)$$

834 which has one global maxima (i.e., $c_{k_0} = 1$ for $k_0 = \arg \min_k d_k$) and multiple local maxima. The
 835 maximum is achieved if and only if $\hat{\mathbf{u}}_{k_0,r} = \pm \hat{\mathbf{v}}_{k_0,r}$ for all r and $\sum_r |\hat{\mathbf{u}}_{k_0,r}|^2 = \sum_r |\hat{\mathbf{v}}_{k_0,r}|^2 = 1/2$.
 836

837 **Local maxima.** For each irreducible representation k_0 , $c_{k_0} = 1$ is a local maxima. This is because
 838 for small perturbation ϵ that moves the solution from $c_k = \mathbb{I}(k = k_0)$ to $c'_k = \begin{cases} 1 - \epsilon & \text{if } k = k_0 \\ \epsilon_k & \text{if } k \neq k_0 \end{cases}$
 839 with $\epsilon_k \geq 0$ and $\sum_{k \neq k_0} \epsilon_k = \epsilon$, for $\mathcal{E} = \mathcal{E}(\{c_k\})$ and $\mathcal{E}' = \mathcal{E}(\{c'_k\})$ we have:
 840

$$841 \mathcal{E}' = \frac{M}{8} \sum_{k \neq 0} \frac{(c'_k)^2}{d_k} = \frac{M}{8} \left(\frac{(c_{k_0} - \epsilon)^2}{d_{k_0}} + \sum_{k \neq k_0, 0} \frac{\epsilon_k^2}{d_k} \right) \quad (22)$$

$$845 \leq \frac{M}{8} \left(\frac{c_{k_0}^2}{d_{k_0}} - \frac{2\epsilon}{d_{k_0}} \right) + O(\epsilon^2) < \frac{M}{8} \frac{c_{k_0}^2}{d_{k_0}} = \frac{M}{8} \sum_{k \neq 0} \frac{c_k^2}{d_k} = \mathcal{E} \quad (23)$$

847 All local maxima are flat, since we can always move around within $\hat{\mathbf{u}}_{k,r}$ and $\hat{\mathbf{v}}_{k,r}$, while the objective
 848 function remains the same. \square
 849

850 **Optimizing in Real domain.** The above analysis uses complex irreducible representations. For real
 851 \mathbf{w} , $\hat{S}_{k,r}$ will be a complex conjugate of $\hat{S}_{-k,r}$ for conjugate irreducible representations k and $-k$.
 852 This means that we can partition the sum in Eqn. 19 into real and complex parts:
 853

$$854 \mathcal{E}(\mathbf{w}) = \frac{M}{2} \sum_{k \neq 0, k \text{ real}} \frac{1}{d_k} \left| \sum_r \text{tr}(\hat{S}_{k,r}) \right|^2 + M \sum_{k \neq 0, k \text{ complex, take one}} \frac{1}{d_k} \left| \sum_r \text{tr}(\hat{S}_{k,r}) \right|^2 \quad (24)$$

856 The above equation holds since R_g is real, and for any complex irreducible representation k , its
 857 conjugate representation $-k$ is also included. Therefore, to optimize \mathcal{E} in the real domain \mathbb{R} , we
 858 can just optimize only on the real part plus the complex part taken one of the conjugate pair in the
 859 complex domain \mathbb{C} .
 860

861 **Zero-meaned one hot representation.** Note that if we use zero-meaned one hot representation
 862 $\tilde{\mathbf{e}}_h = P_1^\perp \mathbf{e}_h$, then $R_{h_1} \tilde{\mathbf{e}}_{h_2} = \tilde{\mathbf{e}}_{h_1 h_2}$ and $P \tilde{\mathbf{e}}_h = \tilde{\mathbf{e}}_{h-1}$ still hold, and $\tilde{X}_h = P_1^\perp X_h = P_1^\perp [R_h^\top, P] =$
 863 $[R_h^\top, P][P_1^\perp; P_1^\perp]$. This means that we can still use X_h but enforce zero-meaned constraints on \mathbf{u}
 and \mathbf{v} , which is already included since $Q^*\mathbf{1} = 0$.

864 **Corollary 1** (Flatness of local maxima of \mathcal{E} for group input). *Local maxima of \mathcal{E} for group arith-
865 metics tasks with $|H| = M > 2$ are flat, i.e., at least one eigenvalue of its Hessian is zero.*
866

867 *Proof.* For Abelian group H with $|H| = M > 2$, all irreducible representations are 1-dimensional,
868 and at least one of it is complex. Since \mathbb{C} is treated as 2D space in optimization, it has at least 1
869 degree of freedom to change without changing its function value (Eqn. 24). So the Hessian has at
870 least 1 zero eigenvalue. For non-Abelian group, there is at least one irreducible representation k with
871 dimension greater than 1, which means it has at least 1 degrees of freedom to change $\hat{S}_{k,r}$ without
872 changing $|\sum_r \text{tr}(\hat{S}_{k,r})|^2$ and thus its function value (Eqn. 24). So the Hessian has at least 1 zero
873 eigenvalue. \square
874

875 A.2 RECONSTRUCTION POWER OF LEARNED FEATURES (SEC. 5.4)
876

877 **Theorem 3** (Target Reconstruction). *Assume (1) \mathcal{E} is optimized in complex domain \mathbb{C} , (2) for each
878 irrep k , there are $m_k^2 d_k^2$ pairs of learned weights $\mathbf{w} = [\mathbf{u}; \pm P\mathbf{u}]$ whose associated rank-1 matrices
879 $\{\mathbf{u}\mathbf{u}^*\}$ form a complete bases for \mathcal{H}_k and (3) the top layer V also learns with $\eta = 0$, then $\hat{Y} = \tilde{Y}$.*
880

881 *Proof.* For each nontrivial irrep k , let Π_k be the central idempotent projector onto the isotypic
882 subspace $\mathcal{H}_k = I_{m_k} \otimes \mathbb{C}^{d_k}$ (for the regular rep, $m_k = d_k$). Let $\text{End}(\mathcal{H}_k)$ be the space of all linear
883 operators that map \mathcal{H}_k to itself. Note that the dimensionality of \mathcal{H}_k is $D_k := m_k d_k$.
884

885 Let $\mathbf{w}_j = [\mathbf{u}_j, P\mathbf{v}_j]$ be the weights learned by optimizing the energy function \mathcal{E} with quadratic
886 activation $\sigma(x) = x^2$. From Thm. 2, we know that at local optima, $\mathbf{u}_j = \pm \mathbf{v}_j$ and $\mathbf{1}^\top \mathbf{u}_j = 0$.
887 Therefore, the feature $\tilde{\mathbf{f}}_{j,h} \in \mathbb{R}^M$ is given by (\circ denotes the Hadamard product)

$$888 \tilde{\mathbf{f}}_{j,h} = \pm 2(R_h^\top \mathbf{u}_j) \circ \mathbf{u}_j + (R_h^\top \mathbf{u}_j) \circ 2 - \frac{1}{M} \sum_h (R_h^\top \mathbf{u}_j) \circ 2$$

891 The third term $\mathbf{u} \circ 2$ is a constant across all h and was removed in the zero-meaned projection. By
892 our assumption we have node j and j' with both positive and negative signs. So $\frac{1}{2}(\tilde{\mathbf{f}}_{j,h} - \tilde{\mathbf{f}}_{j',h}) =$
893 $2(R_h^\top \mathbf{u}_j) \circ \mathbf{u}_j$. If a linear representation of $\{\tilde{\mathbf{f}}_j\}$ can perfectly reconstruct the target \tilde{Y} , so does the
894 original representation. So for now we just let feature $\tilde{\mathbf{f}}_{j,h} = 2(R_h^\top \mathbf{u}_j) \circ \mathbf{u}_j = 2\text{diag}(R_h^\top \mathbf{u}_j \mathbf{u}_j^*)$.
895 Let $U_j := \mathbf{u}_j \mathbf{u}_j^*$, which is Hermitian in $\text{End}(\mathcal{H}_k)$, then $\tilde{\mathbf{f}}_{j,h} = 2\text{diag}(R_h^\top U_j)$.
896

897 **Gram block diagonalization.** For each irrep k , let J_k be the set of all node j that converges to the
898 k -th irrep. For any Hermitian operator U supported in \mathcal{H}_k (i.e. $U = \Pi_k U \Pi_k$), define the centered
899 quadratic cross-feature
900

$$\mathbf{c}_U(h) := 2\text{diag}(R_h^\top U) \in \mathbb{C}^M,$$

902 and write $\mathbf{c}_{U_j} = [\mathbf{c}_{U_j}(h)]_{h \in H} \in \mathbb{C}^{M^2}$ as a concatenated vector.
903

904 For $U, V \in \text{End}(\mathcal{H}_k)$, define $\mathcal{G}(U, V) := \sum_{h \in H} \langle \mathbf{c}_U(h), \mathbf{c}_V(h) \rangle$. On \mathcal{H}_k , $R_h = I_{m_k} \otimes C_k(h)$, so
905 the map $U \mapsto \mathbf{c}_U(h)$ is linear and the bilinear form \mathcal{G} is invariant under $U \mapsto (I \otimes C_k(g))U(I \otimes
906 C_k(g))^*$. By Schur's lemma, $\mathcal{G}(U, V) = \alpha_k \langle U, V \rangle = \alpha_k \text{tr}(UV^*)$ for some scalar α_k . Evaluating
907 on rank-one $U = V$ (or by a direct calculation) gives $\alpha_k = 4$, hence

$$908 \sum_h \langle \mathbf{c}_U(h), \mathbf{c}_V(h) \rangle = 4 \text{tr}(UV^*).$$

910 For $U_j = \mathbf{u}_j \mathbf{u}_j^*$ and $U_\ell = \mathbf{u}_\ell \mathbf{u}_\ell^*$ from \mathcal{H}_k and \mathcal{H}_ℓ with $k \neq \ell$, we have
911

$$912 \sum_h \langle \mathbf{c}_{U_j}(h), \mathbf{c}_{U_\ell}(h) \rangle = 4\mathbf{1}^\top \sum_h \text{diag}(R_h^\top \mathbf{u}_j \mathbf{u}_j^*) \circ \text{diag}(R_h^\top \bar{\mathbf{u}}_\ell \bar{\mathbf{u}}_\ell^*)$$

$$913 = 4\mathbf{1}^\top \sum_h (R_h^\top \mathbf{u}_j) \circ \bar{\mathbf{u}}_\ell \circ R_h^\top \bar{\mathbf{u}}_\ell \circ \mathbf{u}_\ell = 4\mathbf{1}^\top \left[\left(\sum_h R_h \right) (\mathbf{u}_j \circ \bar{\mathbf{u}}_\ell) \right] \circ \bar{\mathbf{u}}_\ell \circ \mathbf{u}_\ell$$

$$914 = 4|\mathbf{u}_j^* \mathbf{u}_\ell|^2$$

918 This means that $\langle \tilde{\mathbf{f}}_j, \tilde{\mathbf{f}}_\ell \rangle = \langle \mathbf{c}_{U_j}, \mathbf{c}_{U_\ell} \rangle = 0$. And thus the Gram matrix $G := \tilde{F}^\top \tilde{F}$ is block diagonal
919 with each block G_k corresponding to an irrep subspace k . Here $G_k \in \mathbb{C}^{N_k \times N_k}$. Note that since
920 we sample $D_k^2 = m_k^2 d_k^2$ weights, then $\{U_j\}_{j \in J_k}$ becomes a complete set of bases (not necessarily
921 orthogonal bases) and thus G_k is invertible.
922

923 **Right-hand side.** For any $U \in \text{End}(\mathcal{H}_k)$,

$$924 \quad r_U(h') = \sum_x \mathbf{c}_U(h')_x = 2 \text{tr}((\Pi_k R_{h'} \Pi_k) U) = 2 \text{tr}((I_{m_k} \otimes C_k(h')) U).$$

925 and we have $[\tilde{\mathbf{f}}_j^\top \tilde{Y}]_{h'} = [\tilde{\mathbf{f}}_j^\top \tilde{Y}]_{h'} = r_{U_j}(h')$.
926

927 **Solve LS.** Now we try to solve the LS problem $GV = \tilde{F}^\top \tilde{Y}$. Due to the block diagonal nature, this
928 can be solved independently for each G_k . Consider $G_k V_k = \tilde{F}_k^\top \tilde{Y}$. Here $\tilde{F}_k = [\tilde{\mathbf{f}}_j]_{j \in J_k}$ collects the
929 subset column J_k from \tilde{F} .
930

931 Therefore, $V_k = G_k^{-1} \tilde{F}_k^\top \tilde{Y}$ and $v_j(h')$ as the (j, h') entry of V_k , has $v_j(h') = \sum_l [G_k^{-1}]_{jl} r_{U_l}(h') =$
932 $2 \sum_l [G_k^{-1}]_{jl} \text{tr}((I_{m_k} \otimes C_k(h')) U_l)$. Then we have $\hat{Y}^{(k)} = \tilde{F}_k V_k$:
933

$$934 \quad \hat{Y}_{(\cdot, h), h'}^{(k)} = \sum_{j \in J_k} v_j(h') \mathbf{c}_{U_j}(h) = 4 \sum_{j \in J_k} \sum_l [G_k^{-1}]_{jl} \text{tr}((I \otimes C_k(h')) U_l) \cdot \text{diag}(R_h^\top U_j).$$

935 By linearity in U and completeness of $\{U_j\}$ (the Hermitian bases span all operators in \mathcal{H}_k), we have
936 for any $A \in \text{End}(\mathcal{H}_k)$:

$$937 \quad 4 \sum_{jl} [G_k^{-1}]_{jl} \text{tr}(AU_l) \text{diag}(R_h^\top U_j) = 4 \text{diag} \left(R_h^\top \left(\sum_{jl} [G_k^{-1}]_{jl} \langle A, U_l \rangle U_j \right) \right) = \text{diag}(R_h^\top A)$$

938 The last equality holds by noticing that $\langle A, U_l \rangle = \text{vec}^*(U_l) \text{vec}(A)$ and thus
939 $4 \sum_{jl} [G_k^{-1}]_{jl} \langle A, U_l \rangle U_j = A$. Take $A = I \otimes C_k(h') = \Pi_k R_{h'} \Pi_k \in \text{End}(\mathcal{H}_k)$, and we
940 have:
941

$$942 \quad \hat{Y}_{(\cdot, h), h'}^{(k)} = \text{diag}(R_h^\top \Pi_k R_{h'} \Pi_k) \quad (h, h' \in H).$$

943 To see why $\hat{Y} = \tilde{Y}$, we have:

$$944 \quad \hat{Y}_{(\cdot, h), h'}^{(k)} = \text{diag}(R_h^\top (\Pi_k R_{h'} \Pi_k)) \Rightarrow \sum_{k \neq 0} \hat{Y}_{(\cdot, h), h'}^{(k)} = \text{diag}(R_h^\top \left(\sum_{k \neq 0} \Pi_k R_{h'} \Pi_k \right)).$$

945 Since $\sum_k \Pi_k = I$ and $\Pi_k R_{h'} = R_{h'} \Pi_k$,

$$946 \quad \sum_{k \neq 0} \Pi_k R_{h'} \Pi_k = R_{h'} - \Pi_0.$$

947 where $\Pi_0 = \frac{1}{M} \mathbf{1}_M \mathbf{1}_M^\top$ is the central idempotent projector onto the trivial irrep. Thus

$$948 \quad \sum_{k \neq 0} \hat{Y}_{(\cdot, h), h'}^{(k)} = \text{diag}(R_h^\top R_{h'}) - \text{diag}(R_h^\top \Pi_0) = \begin{cases} (1 - \frac{1}{M}) \mathbf{1}_M, & h = h', \\ -\frac{1}{M} \mathbf{1}_M, & h \neq h', \end{cases}$$

949 because $\text{diag}(R_h^\top R_{h'}) = \mathbf{1}_M$ iff $h = h'$ and 0 otherwise, while $\text{diag}(R_h^\top \Pi_0) = \frac{1}{M} \mathbf{1}_M$ for all h .
950 Hence $\sum_{k \neq 0} \hat{Y}^{(k)} = P_1^\perp Y = \tilde{Y}$. \square
951

952 **Remark.** The above proof also works for real \mathbf{w} since we can always take a real decomposition of
953 R_h and all the above steps follow.
954

955 **Property of the square term.** With quadratic features the class-centered column for node j and
956 block h decomposes as $\tilde{F} = [A, B]$, where for B each column j (and block h) is $\mathbf{b}_{j,h} := R_h^\top (\mathbf{u}_j^{\circ 2}) -$

972 $\frac{\|\mathbf{u}_j\|_2^2}{M} \mathbf{1}_M$ (the ‘‘square’’ part) and for A each column j (and block h) is $\mathbf{a}_{j,h} := 2(R_h^\top \mathbf{u}_j) \circ \mathbf{u}_j$ (the
 973 ‘‘cross’’ part we discussed above). The vector \mathbf{b}_j is entrywise mean-zero, i.e. $\sum_x \mathbf{b}_j(x) = 0$ for all
 974 h , hence it has zero correlation with any class-centered target column $\tilde{Y}_{(\cdot,h')} \propto \mathbf{1}$: $(\mathbf{b}_{j,h}^\top \tilde{Y})_{h'} =$
 975 $\sum_x \mathbf{b}_{j,h'}(x) = 0$. Moreover, under $\mathbf{1}^\top \mathbf{u}_j = \mathbf{1}^\top \mathbf{u}_\ell = 0$ one has $\sum_h \langle \mathbf{b}_{j,h}, \mathbf{a}_{\ell,h} \rangle = 0$. So the normal
 976 equation becomes
 977
$$\tilde{F}^\top \tilde{F} V = \begin{bmatrix} A^\top A & A^\top B \\ B^\top A & B^\top B \end{bmatrix} V = \begin{bmatrix} A^\top \tilde{Y} \\ B^\top \tilde{Y} \end{bmatrix}$$

 978 which gives
 979
$$\begin{bmatrix} A^\top A & 0 \\ 0 & B^\top B \end{bmatrix} V = \begin{bmatrix} A^\top \tilde{Y} \\ 0 \end{bmatrix}$$

 980 So even with the square term B in \tilde{F} , V will still have zero coefficient on them.

A.3 SCALING LAWS OF MEMORIZATION AND GENERALIZATION (SEC. 5.5)

981 **Theorem 4** (Amount of samples to maintain local optima). *If we select $n \gtrsim d_k^2 M \log(M/\delta)$ data
 982 sample from $H \times H$ uniformly at random, then with probability at least $1 - \delta$, the empirical energy
 983 function $\hat{\mathcal{E}}$ keeps local maxima for d_k -dimensional irreps (Thm. 2).*

984 **Proof. Overview.** We keep the setting and notation of the theorem in the prompt (group H , $|H| = M$, quadratic activation, S as defined there, $z_h = \langle R_h, S \rangle = \text{tr}(R_h^\top S)$, zero-mean removal already folded into \tilde{R}_h). We analyze random row subsampling and show that the empirical objective keeps the same local-maxima structure with $n \gtrsim M \log(M/\delta)$ retained rows.

985 **Setup.** There are M^2 rows indexed by pairs $(h_1, h_2) \in H \times H$, with target $h = h_1 h_2$. For each $h \in H$, exactly M rows map to h ; we index them by $j \in [M]$ after ordering by h_1 as in the proof, and write

$$s_{h,j} := (R_h^\top S)_{jj}, \quad \text{so that} \quad z_h = \sum_{j=1}^M s_{h,j} = \langle R_h, S \rangle.$$

1001 We subsample *rows* independently with keep-probability $p \in (0, 1]$. Let $\xi_{h,j} \in \{0, 1\}$ be the keep
 1002 indicator for the row (h, j) :

$$\Pr(\xi_{h,j} = 1) = p, \quad \text{i.i.d. over } (h, j).$$

1005 The number of kept rows for target h is

$$\hat{m}_h := \sum_{j=1}^M \xi_{h,j} \sim \text{Bin}(M, p), \quad \mathbb{E}[\hat{m}_h] = pM, \quad \text{Var}(\hat{m}_h) = Mp(1-p).$$

1010 **Estimator for z_h .** We use the *linear/unbiased* (Horvitz–Thompson) target-wise estimator

$$\hat{z}_h := \frac{1}{p} \sum_{j=1}^M \xi_{h,j} s_{h,j}. \quad \Rightarrow \quad \mathbb{E}[\hat{z}_h | S] = z_h.$$

1015 Define the diagonal sampling matrix

$$W_h^{\text{HT}} := \text{diag}\left(\frac{\xi_{h,1}}{p}, \dots, \frac{\xi_{h,M}}{p}\right), \quad \text{so} \quad \hat{z}_h = \text{tr}(R_h^\top S W_h^{\text{HT}}) = \langle R_h W_h^{\text{HT}}, S \rangle.$$

1020 **The empirical Gram operator.** Set the normalized per-target weight

$$w_h := \frac{\hat{m}_h}{pM}, \quad \mathbb{E}[w_h] = 1, \quad \text{Var}(w_h) = \frac{1-p}{pM} \leq \frac{1}{pM}.$$

1024 Decompose W_h^{HT} into its mean and zero-mean parts:

$$W_h^{\text{HT}} = w_h I + \Delta_h, \quad \text{tr}(\Delta_h) = 0, \quad \mathbb{E}[\Delta_h | \hat{m}_h] = 0.$$

1026 Therefore

$$1028 \quad \widehat{z}_h = \langle R_h(w_h I + \Delta_h), S \rangle = w_h z_h + \varepsilon_h, \quad \varepsilon_h := \langle R_h \Delta_h, S \rangle, \quad \mathbb{E}[\varepsilon_h | S, \widehat{m}_h] = 0. \quad (25)$$

1030 Using the decomposition

$$1032 \quad z_h = \sum_{k \neq 0} \sum_{r=1}^{m_k} \text{tr}(C_{k,h}^* \widehat{S}_{k,r}) = \sum_{k \neq 0} \sum_{r=1}^{m_k} \text{vec}(\widehat{S}_{k,r})^* \text{vec}(C_{k,h}),$$

1034 we obtain

$$1036 \quad \sum_h \widehat{z}_h^2 = \sum_h (w_h z_h + \varepsilon_h)^2 = \underbrace{\sum_h w_h^2 z_h^2}_{\text{signal}} + 2 \underbrace{\sum_h w_h z_h \varepsilon_h}_{\text{mixed}} + \underbrace{\sum_h \varepsilon_h^2}_{\text{noise}}. \quad (26)$$

1039 The signal term can be written as a quadratic form over irrep blocks:

$$1041 \quad \sum_h w_h^2 z_h^2 = \sum_{(k,r),(k',r')} \text{vec}(\widehat{S}_{k,r})^* \left[\sum_h w_h^2 \text{vec}(C_{k,h}) \text{vec}(C_{k',h})^* \right] \text{vec}(\widehat{S}_{k',r'}). \quad (27)$$

1044 Recall that the full-data operator is

$$1045 \quad \mathsf{A}_{k,k'} := \frac{1}{M} \sum_h \overline{C}_{k',h} \otimes C_{k,h}.$$

1048 and $\text{vec}(C_{k,h}) \text{vec}(C_{k',h})^*$ is just a column and row reshuffling of $\overline{C}_{k',h} \otimes C_{k,h}$. In the following
1049 we will study approximation errors of $\mathsf{A}_{k,k'}$ instead. Let

$$1050 \quad \widehat{\mathsf{A}}_{k,k'}^{(2)} := \frac{1}{M} \sum_h w_h^2 \overline{C}_{k',h} \otimes C_{k,h} \quad \text{and} \quad \widehat{\mathsf{A}}_{k,k'} := \frac{1}{M} \sum_h w_h \overline{C}_{k',h} \otimes C_{k,h}$$

1053 the *second- and first-weighted* empirical Gram operators, respectively. By construction, $\mathbb{E}[\widehat{\mathsf{A}}_{k,k'}] =$
1054 $\mathsf{A}_{k,k'}$ and $\mathbb{E}[\widehat{\mathsf{A}}_{k,k'}^{(2)}] = \mathsf{A}_{k,k'} + \frac{1-p}{pM} \mathsf{A}_{k,k'}$ (a tiny bias of order $1/(pM)$).

1056 **Error bounds for each (k, k') block.** We will control three deviations, uniformly over all (k, k') :

$$1058 \quad \mathbf{E1} : \quad \left\| \widehat{\mathsf{A}}_{k,k'} - \mathsf{A}_{k,k'} \right\|_{\text{op}} \leq c_1 \sqrt{\frac{\log(M/\delta)}{Mp}}, \quad (28)$$

$$1061 \quad \mathbf{E2} : \quad \left\| \widehat{\mathsf{A}}_{k,k'}^{(2)} - \widehat{\mathsf{A}}_{k,k'} \right\|_{\text{op}} \leq c_2 \sqrt{\frac{\log(M/\delta)}{Mp}} + \frac{c'_2}{Mp}, \quad (29)$$

$$1064 \quad \mathbf{E3} : \quad \left| \sum_h w_h z_h \varepsilon_h \right| \leq c_3 \|z\|_2 \sqrt{\frac{M \log(M/\delta)}{p}}, \quad \sum_h \varepsilon_h^2 \leq c_4 \frac{M \log(M/\delta)}{p}, \quad (30)$$

1066 for numerical constants c_i, c'_i , with probability at least $1 - \delta/3$.

1068 **Tool: Matrix Bernstein (self-adjoint dilation form) (Tropp, 2012).** Let $\{X_i\}$ be independent,
1069 mean-zero random $d \times d$ matrices with $\|X_i\| \leq L$ and $\|\sum_i \mathbb{E}[X_i X_i^*]\| \leq v$. Then for all $t > 0$,

$$1071 \quad \Pr \left(\left\| \sum_i X_i \right\| \geq t \right) \leq 2d \exp \left(-\frac{t^2/2}{v + Lt/3} \right),$$

1074 **Proof of (28).** Fix (k, k') and define $B_h := \overline{C}_{k',h} \otimes C_{k,h}$ (unitary, so $\|B_h\| = 1$). Consider

$$1076 \quad X_h := \frac{1}{M} (w_h - 1) B_h, \quad \mathbb{E}[X_h] = 0, \quad \|X_h\| \leq \frac{|w_h - 1|}{M} \leq \frac{1}{M}.$$

1078 We have

$$1079 \quad \mathbb{E}[X_h X_h^*] = \frac{\mathbb{E}[(w_h - 1)^2]}{M^2} B_h B_h^* = \frac{\text{Var}(w_h)}{M^2} I \preceq \frac{1}{pM^3} I.$$

1080 Summing over h gives variance proxy $v \leq M \cdot \frac{1}{pM^3} = \frac{1}{pM^2}$. Since $d \leq M$, with probability at least
 1081 $1 - \delta/3$, Matrix Bernstein yields
 1082

$$1083 \quad \|\widehat{\mathbf{A}}_{k,k'} - \mathbf{A}_{k,k'}\|_{\text{op}} = \left\| \sum_h X_h \right\| \lesssim \sqrt{\frac{\log(M/\delta)}{Mp}},$$

1086 which is (28).
 1087

1088 **Proof of (29).** Write
 1089

$$1090 \quad \widehat{\mathbf{A}}_{k,k'}^{(2)} - \widehat{\mathbf{A}}_{k,k'} = \frac{1}{M} \sum_h (w_h^2 - w_h) B_h = \underbrace{\frac{1}{M} \sum_h ((w_h - 1)^2 + (w_h - 1)) B_h}_{:=\Sigma_1+\Sigma_2}.$$

1094 For Σ_2 we reuse the argument of (28). For Σ_1 , note that $\mathbb{E}[(w_h - 1)^2] = \text{Var}(w_h) \leq 1/(pM)$,
 1095 and $(w_h - 1)^2$ is sub-exponential with scale $\mathcal{O}(1/(pM))$, so matrix Bernstein again gives that with
 1096 probability at least $1 - \delta/3$,
 1097

$$1098 \quad \|\Sigma_1\|_{\text{op}} \lesssim \sqrt{\frac{\log(M/\delta)}{Mp}} + \frac{1}{Mp}.$$

1101 Combining yields (29).
 1102

1103 **Bounds for the mixed and noise terms in (30).** Conditional on S and $\{w_h\}$, the $\{\varepsilon_h\}$ are inde-
 1104 pendent, mean-zero, and
 1105

$$1106 \quad |\varepsilon_h| = |\langle R_h \Delta_h, S \rangle| \leq \|R_h \Delta_h\|_F \|S\|_F \leq \|\Delta_h\|_F \|S\|_F, \quad \mathbb{E}[\varepsilon_h^2 | S, w_h] \lesssim \frac{\|S\|_F^2}{p}.$$

1108 Hence by scalar Bernstein (and Cauchy–Schwarz for the mixed sum),
 1109

$$1110 \quad \left| \sum_h w_h z_h \varepsilon_h \right| \leq \|w\|_\infty \|z\|_2 \|\varepsilon\|_2 \lesssim \|z\|_2 \sqrt{\frac{M \log(M/\delta)}{p}}, \quad \sum_h \varepsilon_h^2 \lesssim \frac{M \log(M/\delta)}{p},$$

1113 with probability at least $1 - \delta/3$, which is (30).
 1114

1115 Combine the above three bounds, we know that with probability at least $1 - \delta$, (28)–(30) hold at the
 1116 same time.
 1117

Stability of local maxima. For the quadratic case (after mean removal), with the collinear and equal
 1118 length \mathbf{u} and \mathbf{v} required by local maxima, \mathcal{E} can be written as a positive semidefinite quadratic in
 1119 the block masses c_k (Eqn. 21):
 1120

$$1121 \quad \mathcal{E}(c) = \frac{M}{8} \sum_{k \neq 0} \frac{c_k^2}{d_k}, \quad \sum_{k \neq 0} c_k = 1, \quad c_k \geq 0.$$

1123 The empirical energy has the form
 1124

$$1125 \quad \widehat{\mathcal{E}}(c) = \frac{M}{8} c^\top (D + E) c + (\text{terms independent of } c),$$

1127 where $D = \text{diag}(1/d_k)$ and E is the symmetric perturbation induced by replacing $\mathbf{A}_{k,k'}$ with $\widehat{\mathbf{A}}_{k,k'}^{(2)}$
 1128 and by the mixed/noise terms. By (28)–(30),
 1129

$$1130 \quad \|E\|_{\text{op}} \lesssim \sqrt{\frac{\log(M/\delta)}{Mp}} + \frac{1}{Mp} \tag{31}$$

1133 with probability at least $1 - \delta$.
 1134

1134 **Directional slope at a vertex (no gap needed).** Consider a pure-irrep vertex $c = \mathbf{e}_a$ and leak ε
 1135 mass to any other coordinate $b \neq a$: $c'_a = 1 - \varepsilon$, $c'_b = \varepsilon$, others 0. Population change:
 1136

$$1137 \Delta\mathcal{E} = \frac{M}{8} \left(\frac{(1 - \varepsilon)^2 - 1}{d_a} + \frac{\varepsilon^2}{d_b} \right) = -\frac{M}{4d_a} \varepsilon + \mathcal{O}(\varepsilon^2).$$

1139 Hence every leakage direction is strictly downhill at rate $\frac{M}{4d_a}$, even if multiple d_k tie. Therefore, a
 1140 first-order approximation of $\Delta\widehat{\mathcal{E}}$ is
 1141

$$1142 \Delta\widehat{\mathcal{E}} = \Delta\mathcal{E} + \frac{M}{8} \Delta(c^\top E c) = -\frac{M}{4d_a} \varepsilon + \mathcal{O}(\varepsilon^2) + \frac{M}{4} \mathcal{O}(\|E\|_{\text{op}} \varepsilon).$$

1144 Therefore $\Delta\widehat{\mathcal{E}} < 0$ for all sufficiently small $\varepsilon > 0$ provided

$$1146 \frac{M}{4} \|E\|_{\text{op}} < \frac{M}{4d_a} \iff \|E\|_{\text{op}} < \frac{1}{d_a}.$$

1148 Combining with (31), a sufficient sampling condition is

$$1149 \sqrt{\frac{\log(M/\delta)}{Mp}} + \frac{1}{Mp} < \frac{1}{Cd_a} \Rightarrow Mp \gtrsim d_a^2 \log \frac{M}{\delta},$$

1152 for a universal numerical constant C . Since the total number of kept rows is $n = pM^2$, this is
 1153 exactly

$$1154 \boxed{n \gtrsim M d_a^2 \log \frac{M}{\delta}}$$

1156 (up to universal constants). Under this condition, with probability at least $1 - \delta$, every
 1157 pure-irrep vertex remains a strict local maximum of the empirical objective (energies shift by
 1158 $\mathcal{O}(\sqrt{\log(M/\delta)/(Mp)})$). When several irreps have the same d_k (tied energies), which one is the
 1159 global maximizer may swap, but the local-maxima set is preserved. \square
 1160

1161 A.4 MEMORIZATION

1163 **Setting.** Fix a group element h . The admissible training pairs are $(g, g^{-1}h)$ for $g \in H$ with
 1164 probabilities $p_g := p_{g, g^{-1}h}$ and a unique maximum at g^* , i.e., $p_{g^*} > p_g$ for all $g \neq g^*$. Let
 1165 $w = [u; v] \in \mathbb{R}^{2M}$ with budget $\|u\|_2^2 + \|v\|_2^2 = 1$. Define the pair-sums $s_g := u_g + v_{g^{-1}h} \geq 0$.
 1166 Then $\sum_g s_g^2 \leq 2$ and the (single-target) objective reduces to
 1167

$$1168 F(s) := \sum_g p_g \sigma(s_g) \quad \text{subject to} \quad s_g \geq 0, \quad \sum_g s_g^2 \leq 2,$$

1170 where $\sigma \in C^1([0, \infty))$ is strictly increasing on $(0, \infty)$. Maximizing the energy \mathcal{E} is equivalent (up
 1171 to a fixed positive factor) to maximizing F .

1172 **Lemma 5** (KKT characterization via $\phi = \sigma'/x$). *Assume $\sigma'(x) > 0$ for $x > 0$, and define $\phi(x) :=$
 1173 $\sigma'(x)/x$ for $x > 0$. Let s^* be an optimal solution. Then there exists $\lambda \geq 0$ such that for each g :*

$$1175 p_g \phi(s_g^*) = 2\lambda, \quad \text{if } s_g^* > 0, \tag{32}$$

1176 *Moreover, the budget is tight: $\sum_g (s_g^*)^2 = 2$ (hence $\lambda > 0$). If ϕ is strictly monotone on $(0, \infty)$,
 1177 then for every active coordinate $s_g^* > 0$,*

$$1179 s_g^* = \phi^{-1} \left(\frac{2\lambda}{p_g} \right). \tag{33}$$

1182 *Proof.* Consider the Lagrangian $L(s, \lambda, \mu) = \sum_g p_g \sigma(s_g) - \lambda(\sum_g s_g^2 - 2) - \sum_g \mu_g s_g$, with $\lambda \geq 0$,
 1183 $\mu_g \geq 0$. Stationarity gives $p_g \sigma'(s_g) - 2\lambda s_g - \mu_g = 0$. If $s_g > 0$, then $\mu_g = 0$ and $p_g \sigma'(s_g) = 2\lambda s_g$,
 1184 i.e., $p_g \phi(s_g) = 2\lambda$. If $s_g = 0$, complementary slackness allows $\mu_g \geq 0$ and the stationarity
 1185 reads $p_g \sigma'(0) - \mu_g = 0$. Interpreting $\phi(0^+) := \lim_{x \downarrow 0} \sigma'(x)/x$ (possibly $+\infty$), the inequality
 1186 $p_g \phi(0^+) \leq 2\lambda$ encodes the fact that activating $s_g > 0$ would violate the KKT balance. Since
 1187 $\sigma' > 0$ and the objective is increasing in each s_g , the budget must be tight at optimum, hence
 1188 $\sum_g s_g^2 = 2$ and $\lambda > 0$. If ϕ is strictly monotone, (32) uniquely determines s_g as in (33). \square

1188
 1189 **Lemma 6** (Memorization vs. spreading by ϕ -monotonicity). *Under the setup above and assuming*
 1190 $\phi(x) = \sigma'(x)/x$ *is continuous on* $(0, \infty)$:

1191 (A) *If ϕ is nondecreasing on $(0, \sqrt{2}]$, then the unique maximizer is the memorization (peaked)*
 1192 *solution*

$$s_{g^*}^* = \sqrt{2}, \quad s_{g \neq g^*}^* = 0,$$

1193 *realized by* $u = \frac{1}{\sqrt{2}}e_{g^*}$, $v = \frac{1}{\sqrt{2}}e_{(g^*)^{-1}h}$.

1194 (B) *If ϕ is strictly decreasing on $(0, \infty)$, then the unique maximizer spreads and is given by*

$$s_g^* = \phi^{-1}\left(\frac{2\lambda}{p_g}\right) \quad (\text{for all } g \text{ with } 2\lambda/p_g < \phi(0^+)),$$

1201 and $s_g^* = 0$ for any g with $2\lambda/p_g \geq \phi(0^+)$ (if $\phi(0^+) < \infty$). The multiplier $\lambda > 0$ is
 1202 uniquely determined by the budget $\sum_g (s_g^*)^2 = 2$. In particular, if $\phi(0^+) = \infty$ (e.g., ReLU
 1203 on $[0, \infty)$: $\phi(x) = 1/x$; SiLU: $\phi(x) = \frac{\text{sigmoid}(x)}{x} + \text{sigmoid}(x)(1 - \text{sigmoid}(x))$), then
 1204 all coordinates are strictly positive and

$$p_i > p_j \implies s_i^* > s_j^* > 0.$$

1208 *Proof.* (A) *Peaking when ϕ is nondecreasing.* Take any feasible s with two positive coordinates
 1209 $s_i \geq s_j > 0$ and $p_i > p_j$. Define a squared-mass transfer preserving $\sum s_g^2$: $s_i(t) := \sqrt{s_i^2 + t}$,
 1210 $s_j(t) := \sqrt{s_j^2 - t}$, and $\Psi(t) := p_i\sigma(s_i(t)) + p_j\sigma(s_j(t))$. Then

$$\Psi'(t) = \frac{1}{2}[p_i\phi(s_i(t)) - p_j\phi(s_j(t))] \geq \frac{1}{2}[(p_i - p_j)\phi(s_j(t))] > 0,$$

1214 because $s_i(t) \geq s_j(t)$ and ϕ is nondecreasing. Hence Ψ increases with t , so any two-support point
 1215 can be strictly improved by pushing mass to the larger p . Iterating this collapse yields the single-
 1216 support boundary $s_{g^*}^* = \sqrt{2}$, others 0. Uniqueness follows from strict inequality and the uniqueness
 1217 of p_{g^*} .

1218 (B) *Spreading when ϕ is strictly decreasing.* By Lemma 5, the optimal active coordinates satisfy
 1219 $p_g\phi(s_g^*) = 2\lambda$. Since ϕ is strictly decreasing, ϕ^{-1} exists and is strictly decreasing, yielding $s_g^* =$
 1220 $\phi^{-1}(2\lambda/p_g)$ on the active set; complementary slackness gives the thresholding when $\phi(0^+) < \infty$.
 1221 The budget $\sum_g (s_g^*)^2 = 2$ fixes λ , and strict monotonicity implies the profile is strictly ordered by
 1222 p_g . \square

1224 **Theorem 5** (Memorization solution). *Let $\phi(x) := \sigma'(x)/x$ and assume $\sigma'(x) > 0$ for $x > 0$. For*
 1225 *group arithmetic tasks, suppose we only collect sample $(g, g^{-1}h)$ for one target h with probability*
 1226 *p_g . Then the global optimal of \mathcal{E} is a memorization solution, either (1) a focused memorization $\mathbf{w} =$*
 1227 $\frac{1}{\sqrt{2}}(\mathbf{e}_{g^*}, \mathbf{e}_{g^{-1}h})$ *for* $g^* = \arg \max p_g$ *if ϕ is nondecreasing, or (2) a spreading memorization with*
 1228 $\mathbf{w} = \frac{1}{2} \sum_g s_g [\mathbf{e}_g, \mathbf{e}_{g^{-1}h}]$, *if ϕ is strictly decreasing. Here $s_g = \phi^{-1}(2\lambda/p_g)$ and λ is determined by*
 1229 $\sum_g s_g^2 = 2$. *No other local optima exist.*

1231 *Proof.* The conclusion follows directly from Thm. 6. \square

1234 **Some discussions.** We know that

- 1236 • For power activations $\sigma(x) = x^q$ ($q \geq 2$) have $\phi(x) = q x^{q-2}$ nondecreasing; Thm. 6(A)
 1237 gives memorization. In all these cases, the peaked solution is realized by even split $u = \frac{1}{\sqrt{2}}e_{g^*}$, $v = \frac{1}{\sqrt{2}}e_{(g^*)^{-1}h}$; any profile s^* can be realized with, e.g., $u_g = v_{g^{-1}h} = s_g^*/2$.
- 1238 • ReLU on $[0, \infty)$: $\sigma(x) = x$, $\phi(x) = 1/x$ strictly decreasing; Thm. 6(B) yields $s^* \propto p$.
- 1239 • SiLU/Swish/Tanh/Sigmoid: ϕ strictly decreasing with $\phi(0^+) = \infty$; Thm. 6(B) gives a
 1240 strictly ordered spread $s_g^* = \phi^{-1}(2\lambda/p_g)$.

1242 **B** INTERACTIVE FEATURE LEARNING (SEC. 6)
 1243

1244 **B.1** FEATURE REPULSION (SEC. 6.1)
 1245

1246 **Theorem 6** (Repulsion of similar features). *The j -th column of $\tilde{F}B$ is given by $[\tilde{F}B]_j = b_{jj}\tilde{\mathbf{f}}_j +$
 1247 $\sum_{l=1}^K b_{jl}\tilde{\mathbf{f}}_l$, where $\text{sign}(b_{jl}) = -\text{sign}(\tilde{\mathbf{f}}_j^\top P_{\eta,-jl}\tilde{\mathbf{f}}_l)$ and $P_{\eta,-jl} := I - \tilde{F}_{-jl}(\tilde{F}_{-jl}^\top \tilde{F}_{-jl} + \eta I)^{-1}\tilde{F}_{-jl}^\top$
 1248 is a projection matrix constructed from \tilde{F}_{-jl} , which is \tilde{F} excluding the l -th and j -th columns.*
 1249

1250 *Proof.* Let $Q := (\tilde{F}^\top \tilde{F} + \eta I)^{-1}$. Without loss of generality (by a column permutation similarity
 1251 that preserves signs of the corresponding inverse entries), reorder columns so that the pair (j, ℓ)
 1252 becomes $(1, 2)$. Write the partition
 1253

$$\tilde{F} = [\tilde{\mathbf{f}}_1 \ \tilde{\mathbf{f}}_2 \ \tilde{F}_r], \quad \tilde{F}_r := \tilde{F}_{-(1,2)} \in \mathbb{R}^{n \times (K-2)}.$$

1254 Then the ridge Gram matrix $G = \tilde{F}^\top \tilde{F} + \eta I_K$ acquires the 2×2 / remainder block form
 1255

$$1256 \quad G = \begin{bmatrix} a & b & \mathbf{u}^\top \\ b & c & \mathbf{v}^\top \\ \mathbf{u} & \mathbf{v} & H \end{bmatrix}, \quad \text{where} \quad a := \tilde{\mathbf{f}}_1^\top \tilde{\mathbf{f}}_1 + \eta, \quad b := \tilde{\mathbf{f}}_1^\top \tilde{\mathbf{f}}_2, \quad \mathbf{u} := \tilde{F}_r^\top \tilde{\mathbf{f}}_1, \\ 1257 \quad c := \tilde{\mathbf{f}}_2^\top \tilde{\mathbf{f}}_2 + \eta, \quad \mathbf{v} := \tilde{F}_r^\top \tilde{\mathbf{f}}_2, \quad H := \tilde{F}_r^\top \tilde{F}_r + \eta I.$$

1258 Because $\eta > 0$, H is positive definite and hence invertible. The inverse of a block matrix is governed
 1259 by the Schur complement. Define the 2×2 Schur complement
 1260

$$1261 \quad S := \begin{bmatrix} a & b \\ b & c \end{bmatrix} - \begin{bmatrix} \mathbf{u}^\top \\ \mathbf{v}^\top \end{bmatrix} H^{-1} [\mathbf{u} \quad \mathbf{v}] = \begin{bmatrix} \alpha & \beta \\ \beta & \gamma \end{bmatrix},$$

1262 where the entries are
 1263

$$1264 \quad \alpha = a - \mathbf{u}^\top H^{-1} \mathbf{u}, \quad \beta = b - \mathbf{u}^\top H^{-1} \mathbf{v}, \quad \gamma = c - \mathbf{v}^\top H^{-1} \mathbf{v}.$$

1265 A standard block inversion formula (e.g., via Schur complements) yields that the top-left 2×2
 1266 block of G^{-1} equals S^{-1} . In particular, the off-diagonal entry of $Q = G^{-1}$ for indices $(1, 2)$ is the
 1267 off-diagonal entry of S^{-1} . Since
 1268

$$1269 \quad S^{-1} = \frac{1}{\alpha\gamma - \beta^2} \begin{bmatrix} \gamma & -\beta \\ -\beta & \alpha \end{bmatrix} \quad \text{with} \quad \alpha\gamma - \beta^2 > 0$$

1270 (because $G \succ 0$ implies $S \succ 0$), we obtain
 1271

$$1272 \quad q_{12} = (S^{-1})_{12} = -\frac{\beta}{\alpha\gamma - \beta^2}.$$

1273 It remains to identify α, β, γ in terms of ridge residuals with respect to \tilde{F}_r . Note that
 1274

$$1275 \quad H = \tilde{F}_r^\top \tilde{F}_r + \eta I \implies \tilde{F}_r H^{-1} \tilde{F}_r^\top = I_n - P_{\eta, r},$$

1276 by the definition $P_{\eta, r} := I - \tilde{F}_r H^{-1} \tilde{F}_r^\top$. Therefore
 1277

$$1278 \quad \alpha = \tilde{\mathbf{f}}_1^\top \tilde{\mathbf{f}}_1 + \eta - \tilde{\mathbf{f}}_1^\top \tilde{F}_r H^{-1} \tilde{F}_r^\top \tilde{\mathbf{f}}_1 = \eta + \tilde{\mathbf{f}}_1^\top (I - \tilde{F}_r H^{-1} \tilde{F}_r^\top) \tilde{\mathbf{f}}_1 = \eta + \tilde{\mathbf{f}}_1^\top P_{\eta, r} \tilde{\mathbf{f}}_1,$$

$$1279 \quad \beta = \tilde{\mathbf{f}}_1^\top \tilde{\mathbf{f}}_2 - \tilde{\mathbf{f}}_1^\top \tilde{F}_r H^{-1} \tilde{F}_r^\top \tilde{\mathbf{f}}_2 = \tilde{\mathbf{f}}_1^\top (I - \tilde{F}_r H^{-1} \tilde{F}_r^\top) \tilde{\mathbf{f}}_2 = \tilde{\mathbf{f}}_1^\top P_{\eta, r} \tilde{\mathbf{f}}_2,$$

$$1280 \quad \gamma = \eta + \tilde{\mathbf{f}}_2^\top P_{\eta, r} \tilde{\mathbf{f}}_2.$$

1281 Substituting these identities into the expression for q_{12} gives
 1282

$$1283 \quad q_{12} = -\frac{\tilde{\mathbf{f}}_1^\top P_{\eta, r} \tilde{\mathbf{f}}_2}{(\eta + \tilde{\mathbf{f}}_1^\top P_{\eta, r} \tilde{\mathbf{f}}_1)(\eta + \tilde{\mathbf{f}}_2^\top P_{\eta, r} \tilde{\mathbf{f}}_2) - (\tilde{\mathbf{f}}_1^\top P_{\eta, r} \tilde{\mathbf{f}}_2)^2}.$$

1284 The denominator is strictly positive (it is the determinant of the positive definite 2×2 matrix S),
 1285 hence
 1286

$$\text{sign}(q_{12}) = -\text{sign}(\tilde{\mathbf{f}}_1^\top P_{\eta, r} \tilde{\mathbf{f}}_2).$$

1296 Undoing the preliminary permutation shows the same formula for the original indices (j, ℓ) , which
 1297 proves the sign claim.
 1298

1299 Finally, since Q is the inverse Gram with ridge, the j -th column of $\tilde{F}Q$ is

$$1300 \quad (1301) \quad (\tilde{F}Q)_{\bullet j} = \sum_{m=1}^K q_{mj} \tilde{\mathbf{f}}_m = q_{jj} \tilde{\mathbf{f}}_j + \sum_{m \neq j} q_{mj} \tilde{\mathbf{f}}_m.$$

1300
 1301 Because q_{mj} has sign opposite to the ridge-residual similarity $\tilde{\mathbf{f}}_m^\top P_{\eta, -m, j} \tilde{\mathbf{f}}_j$, features that are (resid-
 1302 ually) similar to $\tilde{\mathbf{f}}_j$ enter with negative coefficients and hence subtract from $(\tilde{F}Q)_{\bullet j}$ along those di-
 1303 rections—“repelling” similar features and promoting specialization. This completes the proof. \square

1304
 1305
 1306
 1307
 1308 **B.2 TOP-DOWN MODULATION (SEC. 6.2)**

1309
 1310 **Theorem 7** (Top-down Modulation). *For group arithmetic tasks with $\sigma(x) = x^2$, if the hidden layer*
 1311 *learns only a subset \mathcal{S} of irreps, then the backpropagated gradient $G_F \propto (\Phi_{\mathcal{S}} \otimes \mathbf{1}_M)(\Phi_{\mathcal{S}} \otimes \mathbf{1}_M)^* F$*
 1312 *(see proof for the definition of $\Phi_{\mathcal{S}}$), which yields a modified $\mathcal{E}_{\mathcal{S}}$ that only has local maxima on the*
 1313 *missing irreps $k \notin \mathcal{S}$.*

1314
 1315 *Proof.* Fix a nontrivial isotype (irrep) k and we have

$$1316 \quad \hat{Y}_{(\cdot, h), h'}^{(k)} = \text{diag}\left(R_h^\top (\Pi_k R_{h'} \Pi_k)\right).$$

1317
 1318 Since Π_k is central and idempotent, it commutes with $R_{h'}$ and $\Pi_k^2 = \Pi_k$, hence
 1319

$$\Pi_k R_{h'} \Pi_k = \Pi_k R_{h'} = R_{h'} \Pi_k.$$

1320
 1321 Expand the central idempotent in the group algebra using unitary irreps $\{C_k\}$ and characters χ_k :

$$1322 \quad \Pi_k = \frac{d_k}{M} \sum_{g \in H} \overline{\chi_k(g)} R_g = \frac{d_k}{M} \sum_{g \in H} \chi_k(g^{-1}) R_g. \quad (34)$$

1323
 1324 Therefore

$$1325 \quad \Pi_k R_{h'} = \frac{d_k}{M} \sum_{g \in H} \overline{\chi_k(g)} R_g R_{h'} = \frac{d_k}{M} \sum_{g \in H} \overline{\chi_k(g)} R_{gh'}.$$

1326
 1327 Taking the diagonal after the left shift by R_h^\top gives
 1328

$$1329 \quad \text{diag}(R_h^\top (\Pi_k R_{h'})) = \frac{d_k}{M} \sum_{g \in H} \overline{\chi_k(g)} \text{diag}(R_h^\top R_{gh'}).$$

1330
 1331 Since $R_h^\top R_{gh'} = R_{h^{-1}gh'}$, we have
 1332

$$1333 \quad \text{diag}(R_h^\top R_{gh'}) = \begin{cases} \mathbf{1}_M, & h^{-1}gh' = e, \\ \mathbf{0}, & \text{otherwise.} \end{cases}$$

1334
 1335 Only the unique term $g = hh'^{-1}$ survives, so
 1336

$$1337 \quad \text{diag}(R_h^\top (\Pi_k R_{h'})) = \frac{d_k}{M} \overline{\chi_k(hh'^{-1})} \mathbf{1}_M = \frac{d_k}{M} \chi_k(h'^{-1}h) \mathbf{1}_M,$$

1338
 1339 where we used $\overline{\chi_k(a)} = \chi_k(a^{-1})$ for unitary irreps. Consequently,

$$1340 \quad \boxed{\hat{Y}_{(\text{rows for block } h), h'}^{(k)} = \frac{d_k}{M} \chi_k(h'^{-1}h) \mathbf{1}_M.}$$

1341
 1342 Summing over a subset \mathcal{S} of isotypes yields
 1343

$$1344 \quad \hat{Y}_{(\text{rows for block } h), h'} = \sum_{k \in \mathcal{S}} \hat{Y}_{(\text{rows for block } h), h'}^{(k)} = \frac{1}{M} \sum_{k \in \mathcal{S}} d_k \chi_k(h) \overline{\chi_k(h')} \mathbf{1}_M.$$

1350 Since summing over all $k \neq 0$ leads to $\hat{Y} = \tilde{Y}$ (Thm. 3), for the residual $\hat{Y} - \tilde{Y}$ we have
 1351

$$1352 \quad [\hat{Y} - \tilde{Y}]_{(\text{rows for block } h), h'} = \frac{1}{M} \sum_{k \neq 0, k \notin \mathcal{S}} d_k \chi_k(h) \overline{\chi_k(h')} \mathbf{1}_M.$$

1353
 1354 which means that $\hat{Y} - \tilde{Y} = \Phi_{\mathcal{S}} \Phi_{\mathcal{S}}^* \otimes \mathbf{1}_M$, where $\Phi_{\mathcal{S}} := \left[\sqrt{\frac{d_k}{M}} \chi_k(\cdot) \right]_{k \neq 0, k \notin \mathcal{S}} \in \mathbb{C}^{M \times (\kappa(H) - |\mathcal{S}| - 1)}$.
 1355

1356 Since $\tilde{Y} = P_1^\perp \otimes \mathbf{1}_M$, we have:
 1357

$$1358 \quad G_F \propto (\hat{Y} - \tilde{Y}) \tilde{Y}^\top F = (\Phi_{\mathcal{S}} \Phi_{\mathcal{S}}^* \otimes \mathbf{1}_M \mathbf{1}_M^\top) F = (\Phi_{\mathcal{S}} \otimes \mathbf{1}_M) (\Phi_{\mathcal{S}} \otimes \mathbf{1}_M)^* F$$

1360 Therefore, the energy function \mathcal{E} now becomes
 1361

$$1362 \quad \mathcal{E}_{\mathcal{S}} = \frac{1}{2} \|(\Phi_{\mathcal{S}} \otimes \mathbf{1}_M)^* F\|_2^2 = \frac{1}{2} \|\Phi_{\mathcal{S}}^* \mathbf{z}\|_2^2$$

1364 where $\mathbf{z} = [z_h] = [\langle R_h, S \rangle_F] \in \mathbb{C}^M$ defined in Eqn. 12. Computing each row k in $\Phi_{\mathcal{S}}^* \mathbf{z}$ and use the
 1365 property of projection matrix Π_k (Eqn. 34), we have:
 1366

$$1367 \quad [\Phi_{\mathcal{S}}^* \mathbf{z}]_k = \left\langle \sum_{h \in H} \sqrt{\frac{d_k}{M}} \overline{\chi_k(h)} R_h, S \right\rangle = \sqrt{\frac{M}{d_k}} \langle \Pi_k, S \rangle$$

1370 In the Q space, we have $\langle \Pi_k, S \rangle = \sum_{r=1}^{m_k} \text{tr}(\hat{S}_{k,r})$ and therefore
 1371

$$1372 \quad \mathcal{E}_{\mathcal{S}} = \frac{1}{2} \sum_{k \neq 0, k \notin \mathcal{S}} \frac{M}{d_k} |\langle \Pi_k, S \rangle|^2 = \frac{M}{2} \sum_{k \neq 0, k \notin \mathcal{S}} \frac{1}{d_k} \left| \sum_r \text{tr}(\hat{S}_{k,r}) \right|^2$$

1374 which is exactly the same form as the decomposition (Eqn. 19) in Thm. 2 (but a much cleaner
 1375 derivation). Therefore, all the local maxima of $\mathcal{E}_{\mathcal{S}}$ are still in the same form as Thm. 2, but we just
 1376 remove those local maxima that are in isotype/irreps $k \in \mathcal{S}$, and focus on missing ones. \square
 1377

1378 B.3 MUON OPTIMIZERS LEAD TO DIVERSITY (SEC. 6.3)

1380 **Lemma 2** (Muon optimizes the same as gradient flow). *Muon finds ascending direction to maximize
 1381 joint energy $\mathcal{E}_{\text{joint}}(W) = \sum_j \mathcal{E}(\mathbf{w}_j)$ and has critical points iff the original gradient G_W vanishes.*
 1382

1383 *Proof.* Let $G = [\nabla_{\mathbf{w}_1} \mathcal{E}, \nabla_{\mathbf{w}_2} \mathcal{E}, \dots, \nabla_{\mathbf{w}_K} \mathcal{E}]$ be the gradient matrix. Let $G = UDV^\top$ be the singular
 1384 value decomposition. Then Muon direction is $\hat{G} = UV^\top$ and thus the inner product between \hat{G}
 1385 and G is
 1386

$$\langle \hat{G}, G \rangle_F = \text{tr}(\hat{G}^\top G) = \text{tr}(VU^\top UDV^\top) = \text{tr}(D) \geq 0 \quad (35)$$

1387 So Muon always follows the gradient direction and improve the objective. Furthermore, $\langle \hat{G}, G \rangle_F = 0$ iff
 1388 $D = 0$, which means that $G = 0$. So the stationary points of the Muon dynamics and the
 1389 original gradient dynamics are identical. \square
 1390

1391 **Lemma 7** (Proposition of Fréchet / log-Gumbel selection). *Let x_1, \dots, x_n be i.i.d. positive random
 1392 variables with Fréchet(α) CDF*

$$1393 \quad F(x) = \exp(-x^{-\alpha}), \quad x > 0, \quad \alpha > 0,$$

1394 and let $w_1, \dots, w_n > 0$ be fixed weights. Define
 1395

$$1396 \quad i^* = \arg \max_{1 \leq j \leq n} w_j x_j.$$

1397 Then
 1398

$$1399 \quad \Pr(i^* = i) = \frac{w_i^\alpha}{\sum_{j=1}^n w_j^\alpha}, \quad i = 1, \dots, n.$$

1400 In particular, when $\alpha = 1$,
 1401

$$1402 \quad \Pr(i^* = i) = \frac{w_i}{\sum_{j=1}^n w_j}.$$

1404 *Proof.* Set $Y_j := w_j x_j$. For $t > 0$,

$$1406 \quad \Pr\left(\max_j Y_j \leq t\right) = \prod_{j=1}^n F\left(\frac{t}{w_j}\right) = \exp\left(-\sum_{j=1}^n (w_j/t)^\alpha\right).$$

1409 Differentiating gives the density of the maximum:

$$1410 \quad f_{\max}(t) = \frac{d}{dt} \Pr\left(\max_j Y_j \leq t\right) = \left(\sum_{j=1}^n \alpha w_j^\alpha t^{-\alpha-1}\right) \exp\left(-\sum_{j=1}^n (w_j/t)^\alpha\right).$$

1413 The density that “ i achieves the maximum at level t ” is

$$1415 \quad f_{Y_i}(t) \prod_{j \neq i} F\left(\frac{t}{w_j}\right) = \alpha w_i^\alpha t^{-\alpha-1} \exp\left(-\sum_{j=1}^n (w_j/t)^\alpha\right).$$

1418 Hence the conditional probability that i is the argmax given $\max_j Y_j = t$ is

$$1419 \quad \Pr(i^* = i \mid \max_j Y_j = t) = \frac{\alpha w_i^\alpha t^{-\alpha-1}}{\sum_{j=1}^n \alpha w_j^\alpha t^{-\alpha-1}} = \frac{w_i^\alpha}{\sum_{j=1}^n w_j^\alpha},$$

1422 which is independent of t . Averaging over t yields the stated result. \square

1423 **Lemma 8** (The properties of the dynamics in Eqn. 9). *The dynamics always converges to ζ_{l^*} for*
1424 $l^* = \arg \max_l \mu_l \alpha_l(0)$. *That is, the initial leader always win.*

1426 *Proof.* Note that due to orthogonality of $\{\zeta_l\}$, the dynamics can be written as

$$1428 \quad \dot{\alpha}_j = \mu_j \alpha_j^2, \quad \mu_j > 0,$$

1429 with the constraint $\sum_{j=1}^L \alpha_j^2 \leq 1$. Define

$$1431 \quad r_j := \mu_j \alpha_j.$$

1433 **Interior.** In the interior, we have

$$1434 \quad \dot{r}_j = \mu_j \dot{\alpha}_j = \mu_j (\mu_j \alpha_j^2) = r_j^2.$$

1435 For any pair i, k define the ratio

$$1437 \quad \rho_{ik} := \frac{r_i}{r_k}.$$

1438 Its derivative is

$$1440 \quad \dot{\rho}_{ik} = \frac{\dot{r}_i}{r_k} - \frac{r_i}{r_k^2} \dot{r}_k = \frac{r_i^2}{r_k} - \frac{r_i}{r_k^2} r_k^2 = \rho_{ik} (r_i - r_k).$$

1441 Equivalently,

$$1443 \quad \frac{d}{dt} \log \frac{r_i}{r_k} = r_i - r_k. \quad (1)$$

1444 Thus if $r_\ell(0) > r_j(0)$, then $\frac{d}{dt} \log(r_\ell/r_j) > 0$ and $\rho_{\ell j}(t)$ is strictly increasing. Hence a strict leader
1445 in r cannot be overtaken in the interior.

1447 **Boundary region** ($\sum_j \alpha_j^2 = 1$). On the unit sphere, the projected dynamics is

$$1449 \quad \dot{\alpha}_j = \mu_j \alpha_j^2 - \lambda \alpha_j, \quad \lambda = \sum_{k=1}^L \mu_k \alpha_k^3.$$

1452 In terms of r_j ,

$$1453 \quad \dot{r}_j = r_j(r_j - \nu), \quad \nu = \sum_{k=1}^L \alpha_k^2 r_k = \sum_{k=1}^L \frac{r_k^2}{\mu_k^2} r_k.$$

1455 For the ratio $\rho_{ik} = r_i/r_k$ we again obtain

$$1457 \quad \dot{\rho}_{ik} = \rho_{ik} (r_i - r_k) \implies \frac{d}{dt} \log \frac{r_i}{r_k} = r_i - r_k. \quad (2)$$

1458 **Monotonicity of ratios.** From (1)–(2), if $r_\ell(0) > r_j(0)$ then
 1459

$$1460 \quad \frac{d}{dt} \log \frac{r_\ell}{r_j} > 0 \quad \forall t,$$

1462 so $\rho_{\ell j}(t) = r_\ell(t)/r_j(t)$ is strictly increasing for every $j \neq \ell$. Thus a strict leader ℓ remains the
 1463 unique leader for all time.
 1464

1465 **Convergence to the vertex.** Define weights

$$1466 \quad w_j := \alpha_j^2 = \frac{r_j^2}{\mu_j^2}, \quad \sum_j w_j = 1.$$

1469 Their dynamics is
 1470

$$\dot{w}_j = 2w_j(r_j - \nu).$$

1471 Taking ratios,
 1472

$$1473 \quad \frac{d}{dt} \log \frac{w_i}{w_k} = 2(r_i - r_k).$$

1474 In particular, $\frac{w_\ell}{w_j}$ is strictly increasing for every $j \neq \ell$. Therefore
 1475

$$1476 \quad \frac{w_j(t)}{w_\ell(t)} \rightarrow 0 \quad (j \neq \ell),$$

1478 implying $w_\ell(t) \rightarrow 1$ and $w_j(t) \rightarrow 0$. Hence
 1479

$$1480 \quad \alpha(t) \rightarrow \mathbf{e}_\ell \quad \text{as } t \rightarrow \infty.$$

1482 \square

1483 **Lemma 9** (Muon projection). *For the matrix $A = [Q, \mathbf{v}]$ where Q is a column orthonormal matrix
 1484 and \mathbf{v} is a vector with small magnitude, its Muon regulated version $\hat{A} = [\hat{A}_1, \hat{\mathbf{v}}]$ takes the following
 1485 form:*

$$1486 \quad \hat{\mathbf{v}} = \left(\frac{\mathbf{v}_\perp}{\|\mathbf{v}_\perp\|} + \frac{\mathbf{v}_\parallel}{1 + \|\mathbf{v}_\perp\|} \right) + O(\|\mathbf{v}_\perp\|^2) \quad (36)$$

1488 where $\mathbf{v}_\parallel = QQ^\top \mathbf{v}$ and $\mathbf{v}_\perp = I - QQ^\top \mathbf{v}$.
 1489

1490 *Proof.* Given $A = [Q, B]$ with $Q^\top Q = I_k$, write $B = QC + B_\perp$ where $C := Q^\top B \in \mathbb{R}^{k \times m}$ and
 1491 $B_\perp := (I - QQ^\top)B$.
 1492

1493 Let $T := B_\perp^\top B_\perp \succ 0$. For $c > 0$ define

$$1494 \quad \hat{A}^{(c)} = A(A^\top A)^{-1/c}, \quad \hat{A}^{(c)} = [\hat{A}_1^{(c)}, \hat{A}_2^{(c)}].$$

1496 We derive a first-order (in C) formula for the last block $\hat{A}_2^{(c)}$.
 1497

1498 The exact Gram matrix is

$$1499 \quad G := A^\top A = \begin{bmatrix} I_k & C \\ C^\top & C^\top C + T \end{bmatrix} = G_0 + H, \quad G_0 := \text{diag}(I_k, T), \quad H := \begin{bmatrix} 0 & C \\ C^\top & C^\top C \end{bmatrix}.$$

1502 Treat C as small. To first order in C we may drop the quadratic block:

$$1503 \quad H = \begin{bmatrix} 0 & C \\ C^\top & 0 \end{bmatrix} + O(\|C\|^2).$$

1506 **Diagonalizing T .** Let $T = U\Lambda U^\top$ with $\Lambda = \text{diag}(\lambda_1, \dots, \lambda_m)$, $\lambda_j > 0$. Define the block orthogonal
 1507 change of basis
 1508

$$1509 \quad P := \text{diag}(I_k, U) \quad \Rightarrow \quad \tilde{G} := P^\top GP, \quad \tilde{G}_0 := P^\top G_0 P = \text{diag}(I_k, \Lambda), \quad \tilde{H} := P^\top H P = \begin{bmatrix} 0 & \tilde{C} \\ \tilde{C}^\top & 0 \end{bmatrix},$$

1511 where $\tilde{C} := C U$. All first-order statements can be done in this basis and then mapped back by P .

1512 **First-order Taylor Expansion.** Now let's do the Taylor expansion. Write
 1513

$$1514 \quad \tilde{G} = \tilde{G}_0 + \tilde{H} = \tilde{G}_0^{1/2} \left(I + \underbrace{\tilde{G}_0^{-1/2} \tilde{H} \tilde{G}_0^{-1/2}}_{=:E} \right) \tilde{G}_0^{1/2}.$$

1515
 1516 Since $\tilde{G}_0 = \text{diag}(I_k, \Lambda)$,

$$1517 \quad E = \begin{bmatrix} 0 & \tilde{C} \Lambda^{-1/2} \\ \Lambda^{-1/2} \tilde{C}^\top & 0 \end{bmatrix} \quad \text{is } O(\|C\|).$$

1518 For the scalar function $f(x) = x^{-1/c}$,

$$1519 \quad (I + E)^{-1/c} = I - \frac{1}{c} E + O(\|E\|^2).$$

1520 Therefore

$$1521 \quad \tilde{G}^{-1/c} = \tilde{G}_0^{-1/2} (I + E)^{-1/c} \tilde{G}_0^{-1/2} = \tilde{G}_0^{-1/c} - \frac{1}{c} \tilde{G}_0^{-1/2} E \tilde{G}_0^{-1/2} + O(\|C\|^2).$$

1522 Compute the blocks using $\tilde{G}_0^{-1/2} = \text{diag}(I_k, \Lambda^{-1/2})$:

$$1523 \quad \tilde{G}_0^{-1/2} E \tilde{G}_0^{-1/2} = \begin{bmatrix} 0 & \tilde{C} \Lambda^{-1} \\ \Lambda^{-1} \tilde{C}^\top & 0 \end{bmatrix}.$$

1524 Hence, to first order,

$$1525 \quad \tilde{G}^{-1/c} = \begin{bmatrix} I_k & 0 \\ 0 & \Lambda^{-1/c} \end{bmatrix} - \frac{1}{c} \begin{bmatrix} 0 & \tilde{C} \Lambda^{-1} \\ \Lambda^{-1} \tilde{C}^\top & 0 \end{bmatrix} + O(\|C\|^2). \quad (37)$$

1526 **Back to the original space.** Now

$$1527 \quad G^{-1/c} = P \tilde{G}^{-1/c} P^\top.$$

1528 Using (37) and $P = \text{diag}(I_k, U)$,

$$1529 \quad G^{-1/c} = \begin{bmatrix} I_k & 0 \\ 0 & U \Lambda^{-1/c} U^\top \end{bmatrix} - \frac{1}{c} \begin{bmatrix} 0 & C U \Lambda^{-1} U^\top \\ U \Lambda^{-1} U^\top C^\top & 0 \end{bmatrix} + O(\|C\|^2).$$

1530 Since $U \Lambda^{-1} U^\top = T^{-1}$ and $U \Lambda^{-1/c} U^\top = T^{-1/c}$,

$$1531 \quad G^{-1/c} = \begin{bmatrix} I_k & 0 \\ 0 & T^{-1/c} \end{bmatrix} - \frac{1}{c} \begin{bmatrix} 0 & C T^{-1} \\ T^{-1} C^\top & 0 \end{bmatrix} + O(\|C\|^2).$$

1532 Now multiply

$$1533 \quad \hat{A}^{(c)} = [Q, QC + B_\perp] G^{-1/c}.$$

1534 Taking the *last m columns* (the 2nd block) and keeping first-order terms:

$$1535 \quad \hat{A}_2^{(c)} = Q \left(-\frac{1}{c} C T^{-1} \right) + (QC + B_\perp) T^{-1/c} + O(\|C\|^2)$$

$$1536 \quad = B_\perp T^{-1/c} + Q \left(C T^{-1/c} - \frac{1}{c} C T^{-1} \right) + O(\|C\|^2).$$

1537 Factor the Q -part columnwise via the spectral calculus of T . If $T = U \Lambda U^\top$, then on each eigenvalue
 1538 λ the scalar factor is

$$1539 \quad \lambda^{-1/c} - \frac{1}{c} \lambda^{-1} = \frac{1 - \lambda^{1-1/c}}{1 - \lambda}.$$

1540 Thus, in matrix form,

$$1541 \quad C T^{-1/c} - \frac{1}{c} C T^{-1} = C (I - T^{1-1/c}) (I - T)^{-1}.$$

1542 and we have

$$1543 \quad \boxed{\hat{A}_2^{(c)} = B_\perp T^{-1/c} + B_\parallel (I - T^{1-1/c}) (I - T)^{-1} + O(\|C\|^2).} \quad (38)$$

1544 where $B_\parallel = QQ^\top B$.

1545 For polar case $c = 2$, the operator becomes $(I - T^{1/2})(I - T)^{-1}$. For $B = \mathbf{v}$, we have $T = B_\perp^\top B_\perp = \|\mathbf{v}_\perp\|_2^2$ and the conclusion follows. \square

1566 **Lemma 10** (Bound of T_0).

1567

$$1568 T_0 \geq \max \left(\min_{l=1}^L 1/p_l, L \sum_{l=1}^L 1/l \right). \quad (39)$$

1569

1570 *Proof.* $T_0 \geq \min_l 1/p_l$ since the expected time to collect all the coupons is always larger than
1571 collecting the rarest coupon alone.

1572 To prove $T_0 \geq L \sum_{l=1}^L 1/l$, fix $t > 0$ and consider the function

1573

$$1574 h(p) = \log(1 - e^{-pt}), \quad p > 0.$$

1575

1576 A direct computation shows

1577

$$1578 h''(p) = -\frac{t^2}{4 \sinh^2(pt/2)} < 0,$$

1579

1580 so h is concave. By Jensen's inequality and $\sum_i p_i = 1$,

1581

$$1582 \sum_{i=1}^L \log(1 - e^{-p_i t}) \leq L \log(1 - e^{-t/L}).$$

1583

1584 Exponentiating gives the pointwise bound

1585

$$1586 \prod_{i=1}^L (1 - e^{-p_i t}) \leq (1 - e^{-t/L})^L.$$

1587

1588 Therefore

1589

$$1590 \mathbb{E}[T_0] \geq \int_0^\infty \left(1 - (1 - e^{-t/L})^L \right) dt.$$

1591

1592 To evaluate the integral, set $u = e^{-t/L}$, so $dt = -L du/u$ and $t : 0 \rightarrow \infty$ maps to $u : 1 \rightarrow 0$:

1593

$$1594 \int_0^\infty \left(1 - (1 - e^{-t/L})^L \right) dt = L \int_0^1 \frac{1 - (1 - u)^L}{u} du = L \int_0^1 \sum_{l=0}^{L-1} (1 - u)^l du = L \sum_{l=0}^{L-1} \frac{1}{l+1}$$

1595

1596 Thus the conclusion holds. Equality holds if and only if $p_1 = \dots = p_L = 1/L$, since that is the
1597 case of equality in Jensen. \square

1600 **Theorem 8** (Muon rebalances gradient updates). *Consider the following dynamics (Tian, 2023):*

1601

$$1602 \dot{\mathbf{w}} = A(\mathbf{w})\mathbf{w}, \quad \|\mathbf{w}\|_2 \leq 1 \quad (9)$$

1603

1604 where $A(\mathbf{w}) := \sum_l \lambda_l(\mathbf{w}) \zeta_l \zeta_l^\top$. Assume that (1) $\{\zeta_l\}$ form orthonormal bases, (2) for $\mathbf{w} =$
1605 $\sum_l \alpha_l \zeta_l$, we have $\lambda_l(\mathbf{w}) = \mu_l \alpha_l$ with $\mu_l \leq 1$, and (3) $\{\alpha_l\}$ is initialized from inverse-exponential
1606 distribution with $\text{CDF}(x) = \exp(-x^{-a})$ with $a > 1$. Then

- **Independent feature learning.** $\Pr[\mathbf{w} \rightarrow \zeta_l] = p_l := \mu_l^a / \sum_l \mu_l^a$. Then the expected
1607 #nodes to get all local maxima is $T_0 \geq \max \left(1 / \min_l p_l, \sum_{l=1}^L 1/l \right)$.
- **Muon guiding.** If we use Muon optimizer to optimize K nodes sequentially, then the ex-
1608 pected #nodes to get all local maxima is $T_a = 2^{-a} T_0 + (1 - 2^{-a})L$. For large a , $T_a \sim L$.

1610 *Proof.* From Lemma 8, we know that the final mode ζ_l that the nodes converge into is the one with
1611 largest initial α_l :

1612

$$1613 \Pr[\mathbf{w} \rightarrow \zeta_l] = \Pr[l = \arg \max_{l'} \mu_{l'} \alpha_{l'}(0)] \quad (40)$$

1614

1615 By Lemma 7, we have $\Pr[\mathbf{w} \rightarrow \zeta_l] = p_l := \mu_l^a / \sum_l \mu_l^a$.

1616 **Independent feature learning.** In this case, getting all local modes $\{\zeta_l\}$ is identical to the coupon
1617 collector problem with L coupons. With the property of the distribution (Lemma 7), we know that
1618 the probability of getting l -th local maxima is $p_l := \mu_l^a / \sum_l \mu_l^a$.

1620 Therefore, the expected number of trials to collect all local maxima is (Flajolet et al., 1992):
 1621

$$1622 T_0 = \int_0^{+\infty} \left(1 - \prod_{l=1}^L (1 - e^{-p_l t}) \right) dt \quad (41)$$

1625 Note that $T_0 \geq \max \left(1 / \min_l p_l, L \sum_{l=1}^L 1/l \right)$ (Lemma 39). Since each node is independently
 1626 optimized, we need $K \sim T_0$ to collect all local maxima in K hidden nodes with high probability.
 1627

1628 **Muon guiding.** Consider the following setting that we optimize the hidden nodes “incrementally”.
 1629 When learning the weights of node j , we assume all the previous nodes (node 1 to node $j-1$)
 1630 have been learned, i.e., they have converged to one of the ground truth bases $\{\zeta_l\}$, but still keep the
 1631 gradients of them (after deduplication) in the Muon update. Let $S_{j-1} \subseteq [L] = \{1, \dots, L\}$ be the
 1632 subset of local maxima that have been collected.

1633 By Lemma 9, we know that

$$1634 \hat{\mathbf{g}}_j = \frac{1}{\|\mathbf{g}_{j,\perp}\|} \left(\mathbf{g}_{j,\perp} + \frac{\|\mathbf{g}_{j,\perp}\|}{1 + \|\mathbf{g}_{j,\perp}\|} \mathbf{g}_{j,\parallel} \right) + O(\|\mathbf{g}_{j,\perp}\|^2) \quad (42)$$

1637 where $\mathbf{g}_{j,\parallel} = P_{j-1} P_{j-1}^\top \mathbf{g}_j$ and $\mathbf{g}_{j,\perp} = \mathbf{g}_j - \mathbf{g}_{j,\parallel}$. Here $P_{j-1} = [\zeta_s]_{s \in S_{j-1}}$ is the projection matrix
 1638 formed by the previous $j-1$ nodes. Since

$$1639 \|\mathbf{g}_{j,\perp}\| \leq \|\mathbf{g}_j\| = \left\| \sum_l \lambda_l(\alpha_l) \alpha_l \zeta_l \right\| = \left| \sum_l (\lambda_l(\alpha_l) \alpha_l)^2 \right| \leq \left| \sum_l \alpha_l^2 \right| \leq 1 \quad (43)$$

1642 We have $\frac{\|\mathbf{g}_{j,\perp}\|}{1 + \|\mathbf{g}_{j,\perp}\|} \leq 1/2$. Therefore, this means that the parallel components, i.e., the components
 1643 that are duplicated with the previous $j-1$ nodes in the gradient was suppressed by at least $1/2$,
 1644 compared to the orthogonal components (i.e., the directions towards new local maxima). This is
 1645 equivalent to dividing μ_l for all l s that appear in P_{j-1} by (at least) 2. By Lemma 7, for the node j ,
 1646 the probability of converging to a new local maximum other than S_{j-1} is
 1647

$$1648 p_{new, S_{j-1}} \geq \frac{\sum_{l \notin S_{j-1}} p_l}{2^{-a} \sum_{l \in S_{j-1}} p_l + \sum_{l \notin S_{j-1}} p_l} \quad (44)$$

1651 We do this sequentially starting from node j , then node $j+1$, etc. Let $m = |S_{j-1}|$ be the number
 1652 of discovered local maxima. Then the expected time that we find a new local maxima is:

$$1653 \mathbb{E}[\tilde{T}_{m \rightarrow m+1}] = \frac{1}{p_{new, S_{j-1}}} \leq 2^{-a} \mathbb{E}[T_{m \rightarrow m+1}] + 1 - 2^{-a} \quad (45)$$

1656 where $\mathbb{E}[T_{m \rightarrow m+1}] = 1 / \sum_{l \notin S_{j-1}} p_l$ is the expected time for the original coupon collector problem
 1657 to pick a new local maximum, given S_{j-1} known ones. Adding the expected time together, we have

$$1658 T_a = \sum_{m=0}^{L-1} \mathbb{E}[\tilde{T}_{m \rightarrow m+1}] \leq 2^{-a} T_0 + (1 - 2^{-a}) L \quad (46)$$

1661 Note that all the expected time are conditioned on the sequence of known local maxima. But since
 1662 these values are independent of the specific sequence, they are also the expected time overall. \square
 1663

1664 C MORE DETAILED ANALYSIS ON STAGE I (LAZY LEARNING)

1666 To analyze the Stage I more thoroughly, we consider the gradient-flow dynamics of the output layer
 1667 weights V .

1669 Let $\tilde{F} \in \mathbb{R}^{n \times K}$ be a fixed feature matrix and $\tilde{Y} \in \mathbb{R}^{n \times M}$.

1670 We assume throughout that

1672 (A1) \tilde{F} has full column rank K , and

1673 (A2) $\text{col}(\tilde{Y}) \subseteq \text{col}(\tilde{F})$, i.e. there exists $V^* \in \mathbb{R}^{K \times M}$ such that $\tilde{Y} = \tilde{F}V^*$.

- 1674 (A3) Small and independent random initialization on entries of $V(0)$, with mean zero and vari-
 1675 ance α^2 , where $0 < \alpha \ll 1$, and thus $\|V(0)\|_F = O(\alpha\sqrt{KM})$ with high probability.
 1676
 1677 (A4) Zero-mean centering: $\mathbf{1}^\top \tilde{F} = 0$ and $\mathbf{1}^\top \tilde{Y} = 0$.

1678 Note that (A4) is optional. It simplifies some interpretations but is not needed for the main analysis.
 1679

1680 We train a linear readout $V \in \mathbb{R}^{K \times M}$ by minimizing

$$1682 \quad J(V) = \frac{1}{2}(\|\tilde{Y} - \tilde{F}V\|_F^2 + \eta\|V\|_F^2), \quad \eta \geq 0. \quad (47)$$

1684 We define the (matrix) prediction error and the backpropagated gradient $G_{\tilde{F}}$ as

$$1685 \quad E(t) := \tilde{Y} - \tilde{F}V(t) \in \mathbb{R}^{n \times M}, \quad G_{\tilde{F}}(t) := E(t)V(t)^\top \in \mathbb{R}^{n \times K}. \quad (48)$$

1687 Note that in the main text, we use G_F to denote the backpropagated gradient on the uncentered
 1688 feature matrix F , i.e., $G_F = P_1^\perp G_{\tilde{F}}$, where $P_1^\perp := I - \mathbf{1}\mathbf{1}^\top/n$ is the zero-mean projection matrix
 1689 along the sample dimension. As we will see below, the leading term of $G_{\tilde{F}}$ is $\tilde{Y}\tilde{Y}^\top \tilde{F}$ and thus
 1690

$$1691 \quad G_F = P_1^\perp G_{\tilde{F}} \propto P_1^\perp \tilde{Y}\tilde{Y}^\top \tilde{F} = \tilde{Y}\tilde{Y}^\top \tilde{F} = \tilde{Y}\tilde{Y}^\top F. \quad (49)$$

1692 because $\mathbf{1}^\top \tilde{F} = 0$ and $\mathbf{1}^\top \tilde{Y} = 0$.
 1693

1694 We consider continuous-time gradient flow for V :

$$1696 \quad \frac{dV(t)}{dt} = -\nabla_V J(V(t)). \quad (50)$$

1698 The gradient of J with respect to V is
 1699

$$1700 \quad \nabla_V J(V) = \tilde{F}^\top (\tilde{F}V - \tilde{Y}) + \eta V = AV - B, \quad A := \tilde{F}^\top \tilde{F} + \eta I_K, \quad B := \tilde{F}^\top \tilde{Y}. \quad (51)$$

1702 We study the *gradient flow* dynamics

$$1704 \quad \frac{dV}{dt} = -\nabla_V J(V) = -AV + B. \quad (52)$$

1706 Define the error matrix and the backpropagated gradient on \tilde{F} by
 1707

$$1708 \quad E(t) := \tilde{Y} - \tilde{F}V(t) \in \mathbb{R}^{n \times M}, \quad G_{\tilde{F}}(t) := E(t)V(t)^\top \in \mathbb{R}^{n \times K}.$$

1710 Our goal is to understand:

- 1711 1. the *small-time expansion* of $G_{\tilde{F}}(t)$ and show that the leading term is $\tilde{Y}\tilde{Y}^\top \tilde{F}$; and
 1712 2. the *long-time decay* behavior of $G_{\tilde{F}}(t)$, for both $\eta = 0$ and $\eta > 0$.
 1713

1714 C.1 THE DYNAMICS OF $G_{\tilde{F}}$ AT INITIAL TIME STAMPS

1716 C.1.1 SMALL-TIME EXPANSION AND LEADING TERM

1718 Write the Taylor expansions at $t = 0$ as

$$1720 \quad V(t) = V_0 + tV_1 + O(t^2), \quad E(t) = E_0 + tE_1 + O(t^2),$$

1721 where $V_0 := V(0)$ and $E_0 := \tilde{Y} - \tilde{F}V_0$. From (52),
 1722

$$1723 \quad V_1 = \frac{dV}{dt} \Big|_{t=0} = -AV_0 + B = -(\tilde{F}^\top \tilde{F} + \eta I_K)V_0 + \tilde{F}^\top \tilde{Y}. \quad (53)$$

1725 Differentiating $E(t) = \tilde{Y} - \tilde{F}V(t)$ gives
 1726

$$1727 \quad E_1 = \frac{dE}{dt} \Big|_{t=0} = -\tilde{F}V_1 = \tilde{F}(\tilde{F}^\top \tilde{F} + \eta I_K)V_0 - \tilde{F}\tilde{F}^\top \tilde{Y}. \quad (54)$$

1728 Now expand $G_{\tilde{F}}(t)$:
 1729

$$1730 G_{\tilde{F}}(t) = E(t)V(t)^\top = (E_0 + tE_1)(V_0 + tV_1)^\top + O(t^2) = E_0V_0^\top + t(E_0V_1^\top + E_1V_0^\top) + O(t^2).$$

1731 Using $E_0 = \tilde{Y} - \tilde{F}V_0$ and V_1 from (53),
 1732

$$1733 E_0V_1^\top = (\tilde{Y} - \tilde{F}V_0)(-V_0^\top(\tilde{F}^\top\tilde{F} + \eta I_K) + \tilde{Y}^\top\tilde{F}) \\ 1734 = \tilde{Y}\tilde{Y}^\top\tilde{F} - \tilde{F}V_0\tilde{Y}^\top\tilde{F} - \tilde{Y}V_0^\top(\tilde{F}^\top\tilde{F} + \eta I_K) + \tilde{F}V_0V_0^\top(\tilde{F}^\top\tilde{F} + \eta I_K).$$

1735 Every term except $\tilde{Y}\tilde{Y}^\top\tilde{F}$ contains (at least one factor of) V_0 , hence is $O(\alpha)$ in Frobenius norm.
 1736 Moreover, $E_1V_0^\top$ also contains V_0 :
 1737

$$1738 E_1V_0^\top = \tilde{F}(\tilde{F}^\top\tilde{F} + \eta I_K)V_0V_0^\top - \tilde{F}\tilde{F}^\top\tilde{Y}V_0^\top,$$

1739 so $\|E_1V_0^\top\|_F = O(\alpha)$ as well.
 1740

1741 We therefore obtain the small-time expansion

$$1742 G_{\tilde{F}}(t) = \underbrace{\tilde{Y}V_0^\top}_{O(\alpha)} + t\tilde{Y}\tilde{Y}^\top\tilde{F} + tR_1(V_0) + O(t^2), \quad (55)$$

1743 where $R_1(V_0)$ collects all order- t terms that contain V_0 and thus satisfy $\|R_1(V_0)\|_F = O(\alpha)$.
 1744

1745 C.1.2 WHY $\tilde{Y}\tilde{Y}^\top\tilde{F}$ IS THE LEADING TERM

1746 We now compare the deterministic term $\tilde{Y}\tilde{Y}^\top\tilde{F}$ to the V_0 -dependent terms using norm inequalities.
 1747

1748 **Lemma 11** (Lower bound on $\|\tilde{Y}\tilde{Y}^\top\tilde{F}\|_F$). *Let \tilde{F} have full column rank and \tilde{Y} be nonzero. Then*

$$1751 \|\tilde{Y}\tilde{Y}^\top\tilde{F}\|_F \geq \sigma_{\min}(\tilde{F}) \|\tilde{Y}\tilde{Y}^\top\|_F > 0,$$

1752 where $\sigma_{\min}(\tilde{F})$ is the smallest singular value of \tilde{F} .
 1753

1754 *Proof.* For any matrices A, B , $\|AB\|_F^2 = \text{tr}(BB^\top A^\top A)$. Take $A = \tilde{Y}\tilde{Y}^\top$, $B = \tilde{F}$. Since BB^\top is
 1755 PSD with eigenvalues bounded below by $\sigma_{\min}(\tilde{F})^2$,
 1756

$$1757 \|AB\|_F^2 = \text{tr}(BB^\top A^\top A) \geq \sigma_{\min}(\tilde{F})^2 \text{tr}(A^\top A) = \sigma_{\min}(\tilde{F})^2 \|A\|_F^2.$$

1758 Taking square roots gives the result. \square
 1759

1760 Next, bound the V_0 -dependent part. For concreteness, consider the term $\tilde{F}\tilde{F}^\top\tilde{Y}V_0^\top$ (other mixed
 1761 terms are bounded similarly). Using $\|AB\|_F \leq \|A\|_F\|B\|_F$,
 1762

$$1763 \|\tilde{F}\tilde{F}^\top\tilde{Y}V_0^\top\|_F \leq \|\tilde{F}\tilde{F}^\top\tilde{Y}\|_F\|V_0\|_F.$$

1764 Under the iid initialization with variance α^2 , $\|V_0\|_F = O(\alpha\sqrt{KM})$, hence
 1765

$$1766 \|\tilde{F}\tilde{F}^\top\tilde{Y}V_0^\top\|_F = O(\alpha).$$

1767 The same argument applies to all other V_0 -dependent order- t terms in $R_1(V_0)$.
 1768

1769 Combining Lemma 11 with these upper bounds yields

$$1770 \frac{\|R_1(V_0)\|_F}{\|\tilde{Y}\tilde{Y}^\top\tilde{F}\|_F} \leq C(\tilde{F}, \tilde{Y}, K, M) \alpha$$

1771 for some constant C independent of α . Thus, in the limit $\alpha \rightarrow 0$ (small random initialization), the
 1772 term $\tilde{Y}\tilde{Y}^\top\tilde{F}$ is the unique leading contribution at order t .
 1773

1774 **Proposition 2** (Small-time leading term of $G_{\tilde{F}}$). *Under assumptions (A1)–(A2) and small random
 1775 initialization with scale $\alpha \ll 1$,*

$$1777 G_{\tilde{F}}(t) = \tilde{Y}V_0^\top + t\tilde{Y}\tilde{Y}^\top\tilde{F} + O(t\alpha + t^2)$$

1778 in Frobenius norm. In particular, as $\alpha \rightarrow 0$,

$$1779 \frac{G_{\tilde{F}}(t) - \tilde{Y}V_0^\top}{t} \rightarrow \tilde{Y}\tilde{Y}^\top\tilde{F}, \quad \text{and} \quad \|G_{\tilde{F}}(t)\|_F \sim t \|\tilde{Y}\tilde{Y}^\top\tilde{F}\|_F$$

1780 for fixed small t , independently of whether $\eta = 0$ or $\eta > 0$.
 1781

1782 **Remark on the role of η .** The weight decay parameter η only appears in products involving V_0 ,
 1783 and hence all η -dependent order- t contributions are also $O(\alpha)$ in norm. Therefore the leading
 1784 deterministic term $\tilde{Y}\tilde{Y}^\top\tilde{F}$ is the same for both $\eta = 0$ and $\eta > 0$.
 1785

1786 **C.2 LONG-TIME DECAY OF $G_{\tilde{F}}$**

1788 We now analyze the behavior of $G_{\tilde{F}}(t)$ as $t \rightarrow \infty$, again for both $\eta = 0$ and $\eta > 0$.
 1789

1790 **C.2.1 GENERAL SOLUTION OF THE GRADIENT FLOW**

1791 From (52), the gradient flow is a linear ODE with constant coefficients. The unique fixed point V^*
 1792 satisfies

$$1793 \quad AV^* = B \quad \Rightarrow \quad V^* = A^{-1}B.$$

1794 Define $\Delta V(t) := V(t) - V^*$. Then

$$1795 \quad \frac{d}{dt}\Delta V(t) = -A\Delta V(t), \quad \Delta V(t) = e^{-At}\Delta V(0),$$

1797 and hence

$$1798 \quad V(t) = e^{-At}(V(0) - V^*) + V^*. \quad (56)$$

1800 Let $\lambda_{\min}(A)$ denote the smallest eigenvalue of A . Since $A \succeq \tilde{F}^\top\tilde{F}$ and \tilde{F} has full column rank,
 1801 $\lambda_{\min}(A) \geq \sigma_{\min}(\tilde{F})^2$ for $\eta = 0$ and $\lambda_{\min}(A) \geq \sigma_{\min}(\tilde{F})^2 + \eta$ for $\eta > 0$. Standard bounds on
 1802 matrix exponentials give

$$1803 \quad \|\Delta V(t)\|_F \leq e^{-\lambda_{\min}(A)t} \|\Delta V(0)\|_F. \quad (57)$$

1804 The error satisfies

$$1805 \quad E(t) = \tilde{Y} - \tilde{F}V(t) = \tilde{Y} - \tilde{F}V^* - \tilde{F}\Delta V(t) =: E^* - \tilde{F}\Delta V(t),$$

1806 where $E^* := \tilde{Y} - \tilde{F}V^*$ is the residual at the minimizer. Using $\|\tilde{F}\Delta V(t)\|_F \leq \|\tilde{F}\|_2\|\Delta V(t)\|_F$
 1807 and (57),

$$1808 \quad \|E(t) - E^*\|_F \leq \|\tilde{F}\|_2 e^{-\lambda_{\min}(A)t} \|\Delta V(0)\|_F. \quad (58)$$

1810 **C.2.2 CASE $\eta = 0$**

1812 When $\eta = 0$, we have $A = \tilde{F}^\top\tilde{F}$. By assumption (A2), $\tilde{Y} = \tilde{F}V^*$ is exactly realized by the model,
 1813 so $E^* = 0$, i.e.

$$1814 \quad \lim_{t \rightarrow \infty} E(t) = 0.$$

1815 Equations (57) and (58) imply exponential decay:

$$1817 \quad \|V(t) - V^*\|_F \leq e^{-\sigma_{\min}(\tilde{F})^2 t} \|V(0) - V^*\|_F, \quad \|E(t)\|_F \leq \|\tilde{F}\|_2 e^{-\sigma_{\min}(\tilde{F})^2 t} \|V(0) - V^*\|_F.$$

1818 We can now bound $G_{\tilde{F}}(t)$:

$$1819 \quad G_{\tilde{F}}(t) = E(t)V(t)^\top,$$

1821 so

$$1822 \quad \|G_{\tilde{F}}(t)\|_F \leq \|E(t)\|_F \|V(t)\|_2 \leq \|E(t)\|_F (\|V^*\|_2 + \|V(t) - V^*\|_2). \quad (59)$$

1823 Using the exponential bounds above and the fact that $\|V(t) - V^*\|_2 \leq \|V(t) - V^*\|_F$, we obtain

$$1824 \quad \|G_{\tilde{F}}(t)\|_F \leq C_0 e^{-\sigma_{\min}(\tilde{F})^2 t}$$

1825 for some constant C_0 depending on \tilde{F} , V^* and $V(0)$ but not on t .
 1826

1827 Thus in the realizable, unregularized case, the backpropagated gradient decays exponentially to zero.

1828 **Proposition 3** (Exponential decay of $G_{\tilde{F}}$ for $\eta = 0$). *Assume (A1)–(A2) and $\eta = 0$. Then*

$$1829 \quad \lim_{t \rightarrow \infty} G_{\tilde{F}}(t) = 0,$$

1830 and there exists $C_0 > 0$ such that

$$1831 \quad \|G_{\tilde{F}}(t)\|_F \leq C_0 e^{-\sigma_{\min}(\tilde{F})^2 t} \quad \text{for all } t \geq 0.$$

1833 A more refined analysis using the SVD $\tilde{F} = U\Sigma W^\top$ shows that every singular direction of $G_{\tilde{F}}(t)$ is
 1834 a finite linear combination of exponentials $e^{-(\sigma_i^2 + \sigma_{i'}^2)t}$ and $e^{-\sigma_i^2 t}$, so the slowest rate in the Frobenius
 1835 norm is indeed $e^{-\sigma_{\min}(\tilde{F})^2 t}$.

1836 C.2.3 CASE $\eta > 0$
18371838 When $\eta > 0$, the minimizer $V^* = A^{-1}\tilde{F}^\top\tilde{Y}$ is the ridge solution. In general it does *not* exactly
1839 interpolate \tilde{Y} , and the residual

1840
$$E^* := \tilde{Y} - \tilde{F}V^*$$

1841 is nonzero. Consequently the limiting backpropagated gradient
1842

1843
$$G_{\tilde{F}}^* := \lim_{t \rightarrow \infty} G_{\tilde{F}}(t) = E^*V^{*\top}$$

1844

1845 is also nonzero in general.

1846 To study the convergence, write
1847

1848
$$G_{\tilde{F}}(t) - G_{\tilde{F}}^* = E(t)V(t)^\top - E^*V^{*\top} = (E(t) - E^*)V(t)^\top + E^*(V(t) - V^*)^\top.$$

1849 Using (57)–(58) and $\|AB\|_F \leq \|A\|_F\|B\|_2$, we obtain
1850

1851
$$\begin{aligned} \|G_{\tilde{F}}(t) - G_{\tilde{F}}^*\|_F &\leq \|E(t) - E^*\|_F\|V(t)\|_2 + \|E^*\|_F\|V(t) - V^*\|_2 \\ &\leq \left(\|\tilde{F}\|_2\|V(0) - V^*\|_F\|V(t)\|_2 + \|E^*\|_F\|V(0) - V^*\|_F\right)e^{-\lambda_{\min}(A)t}. \end{aligned}$$

1852

1853 Since $\|V(t)\|_2$ is bounded (it converges to $\|V^*\|_2$), this shows exponential convergence of $G_{\tilde{F}}(t)$ to
1854 $G_{\tilde{F}}^*$. Therefore, we have the following proposition:
18551856 **Proposition 4** (Exponential convergence of $G_{\tilde{F}}$ for $\eta > 0$). *Assume (A1)–(A2) and $\eta > 0$. Then*
1857

1858
$$\lim_{t \rightarrow \infty} G_{\tilde{F}}(t) = G_{\tilde{F}}^* := E^*V^{*\top} \neq 0 \text{ in general,}$$

1859

1860 and there exists $C_1 > 0$ such that
1861

1862
$$\|G_{\tilde{F}}(t) - G_{\tilde{F}}^*\|_F \leq C_1 e^{-\lambda_{\min}(A)t}, \quad \lambda_{\min}(A) \geq \sigma_{\min}(\tilde{F})^2 + \eta.$$

1863 Finally, note that
1864

1865
$$G_{\tilde{F}}^* = E^*V^{*\top} = P_\eta \tilde{Y} V^{*\top} = \eta(\tilde{F}\tilde{F}^\top + \eta I)^{-1}\tilde{Y}\tilde{Y}^\top\tilde{F}(\tilde{F}^\top\tilde{F} + \eta I)^{-1} \quad (60)$$

1866

1867 where $P_\eta := I - \tilde{F}(\tilde{F}^\top\tilde{F} + \eta I)^{-1}\tilde{F}^\top = \eta(\tilde{F}\tilde{F}^\top + \eta I)^{-1}$, by Woodbury matrix formula.
18681869 **Summary.**

- 1870 • For small
- t
- , the leading term in
- $G_{\tilde{F}}(t)$
- is
- $t\tilde{Y}\tilde{Y}^\top\tilde{F}$
- , independent of
- η
- . All other terms
-
- 1871 (including those involving
- $V(0)$
- and
- η
-) are lower order in the initialization scale
- α
- .
-
- 1872 • For
- $\eta = 0$
- and realizable
- $\tilde{Y} \in \text{col}(\tilde{F})$
- , both the error
- $E(t)$
- and
- $G_{\tilde{F}}(t)$
- decay exponentially
-
- 1873 to zero at rate at least
- $\sigma_{\min}(\tilde{F})^2$
- .
-
- 1874 • For
- $\eta > 0$
- ,
- $E(t)$
- and
- $V(t)$
- converge exponentially to
- (E^*, V^*)
- , and
- $G_{\tilde{F}}(t)$
- converges
-
- 1875 exponentially to a nonzero limit
- $G_{\tilde{F}}^* = E^*V^{*\top}$
- .
-
- 1876

1877 **D WHEN DOES GROKKING HAPPEN?**
18781879 Previous empirical works show that many hyperparameters can lead to grokking behaviors. Here
1880 we summarize these key factors can be explained through their interactions with G_F and the feature
1881 learning process. Here we categorize these factors into several categories.
18821883 **Learning rate.** (Gromov, 2023) reports that grokking happens without regularization, but with a
1884 large initial learning rate (verified by the author). This corresponds to increasing the strength of
1885 $G_F(t) \propto t\tilde{Y}\tilde{Y}^\top F$ at the initial phase of learning so that the hidden layers receives enough correct
1886 gradient signal.
18871888 **Loss function.** (Prieto et al., 2025) uses stable softmax (linear form) rather than regular softmax
1889 (exponential form) in computing probability. This prevents the model from overfitting to the label
1890 too quickly, and thus maintains a nonzero backpropagated gradient that can be useful for feature

1890 learning. (Kumar et al., 2024) also reports that grokking happens without regularization, using
 1891 vanilla SGD optimizer. Our explanation is that it may take longer for SGD to converge to V_{ridge}
 1892 than Adam, and during that period, the hidden layer has already accumulated a sufficient amount of
 1893 correct gradient signal.

1894 **Weight initialization.** (Liu et al., 2023) reports that grokking happens with small initialization,
 1895 regardless of the weight decay. This is straightforward from our framework, since $G_F(t) = O(\alpha) +$
 1896 $t\tilde{Y}\tilde{Y}^\top F + O(\alpha t) + O(t^2)$ and if the weight initialization α is small, then $G_F(t)$ is dominated by
 1897 clear signal term $t\tilde{Y}\tilde{Y}^\top \tilde{F}$, which leads to grokking. If α is large, then $O(\alpha)$ term is large and the
 1898 initial phase of G_F contains too much noise, and we need to rely on the signal provided by the
 1899 convergence phrase of G_F controlled by the weight decay η . This is consistent with the finding
 1900 by (Liu et al., 2023) that for large weight initialization, regularization is needed for grokking to
 1901 happen, and small regularization leads to slow grokking transition.

1902 **Scaling factor β of the output.** (Kumar et al., 2024; Chizat et al., 2019) reports that scaling the
 1903 output by a factor $\beta > 1$ will make the grokking faster. From Li_2 framework, this corresponds to
 1904 optimizing $J_\beta(V) = \|\tilde{Y} - \beta\tilde{F}V\|_F^2 + \eta\|V\|_F^2$. Following a similar derivation as in Sec. C, we can
 1905 show that at the initial phase, the backpropagated gradient $G_F(t) = O(\alpha) + t\beta\tilde{Y}\tilde{Y}^\top \tilde{F} + O(\alpha\beta t) +$
 1906 $O(t^2)$. So if $\beta > 1$ is large then the signal term $t\beta\tilde{Y}\tilde{Y}^\top \tilde{F}$ becomes more dominant than the case of
 1907 $\beta = 1$, and the grokking happens faster.

1908 **Weight decay η .** According to Eqn. 4, since $G_F(+\infty) \propto \eta\tilde{Y}\tilde{Y}^\top F$, it is clear that the weight decay
 1909 η becomes the *learning rate* of feature learning process. This coincides with findings in empirical
 1910 works (Power et al., 2022; Clauw et al., 2024) that low regularization leads to slow grokking transi-
 1911 tion. This is also consistent with $t \sim 1/\eta$ laws to start grokking (Liu et al., 2023) or reach maximal
 1912 test performance (Lewkowycz & Gur-Ari, 2020).

1913 **Data size n .** Our sample analysis (Theorem. 4) shows the local maxima can be kept with sufficient
 1914 number of samples ($n \gtrsim M \log M$). Intuitively, more samples lead to better shaped local maxima
 1915 with less noise and thus the feature learning is faster.

1916 **The number of hidden nodes K .** Our analysis requires that we need a decent number of hidden
 1917 nodes K to cover the diverse set of the local maxima of \mathcal{E} . On the other hand, Lemma 1 tells that
 1918 very large K may reduce $|G_F(+\infty)|$ and makes grokking slower. This is consistent with the finding
 1919 by (Chizat et al., 2019).

1922 E MORE EXPERIMENTS

1924 E.1 USE GROUPS ALGORITHMS PROGRAMMING (GAP) TO GET NON-ABELIAN GROUPS

1926 GAP (<https://www.gap-system.org/>) is a programming language with a library of thou-
 1927 sands of functions to create and manipulate group. Using GAP, one can easily enumerate all non-
 1928 abelian group of size $M \leq 127$ and create their multiplication tables, which is what we have done
 1929 here. From these non-Abelian groups, for each group size M , we pick one for our scaling law
 1930 experiments (Fig. 4 bottom right) with $\max_k d_k = 2$.

1931
 1932
 1933
 1934
 1935
 1936
 1937
 1938
 1939
 1940
 1941
 1942
 1943

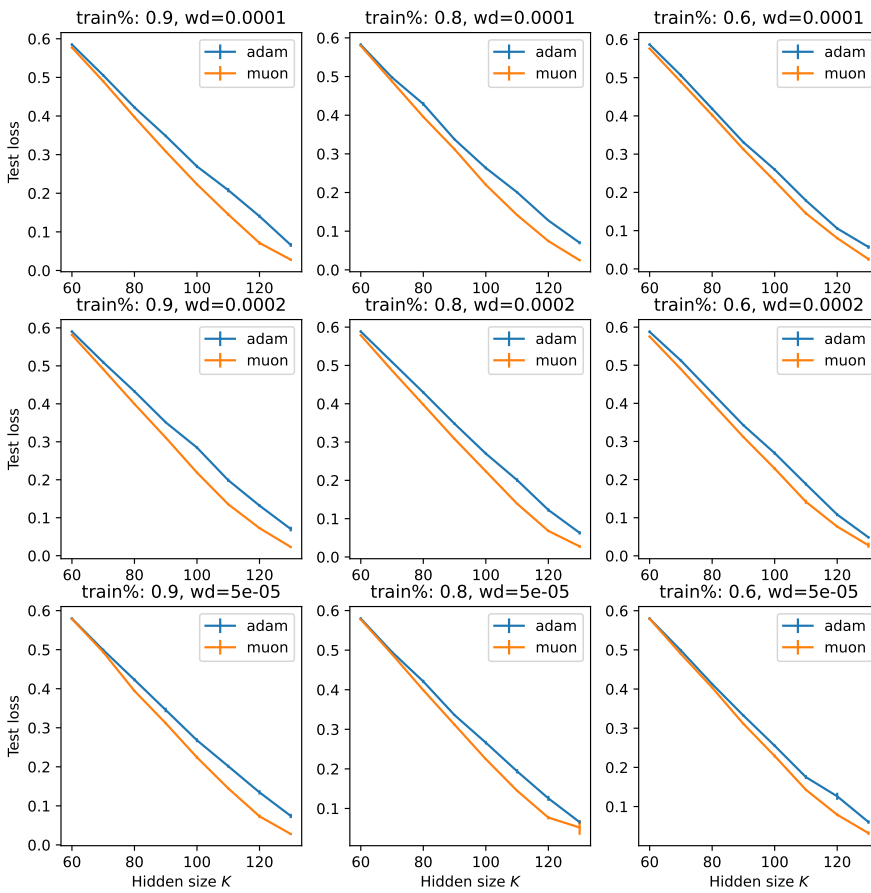


Figure 7: Adam versus Muon optimizers in modular addition tasks with $M = 71$, when the number of hidden nodes K is relatively small compared to M . Muon optimizer achieves lower test loss compared to Adam.

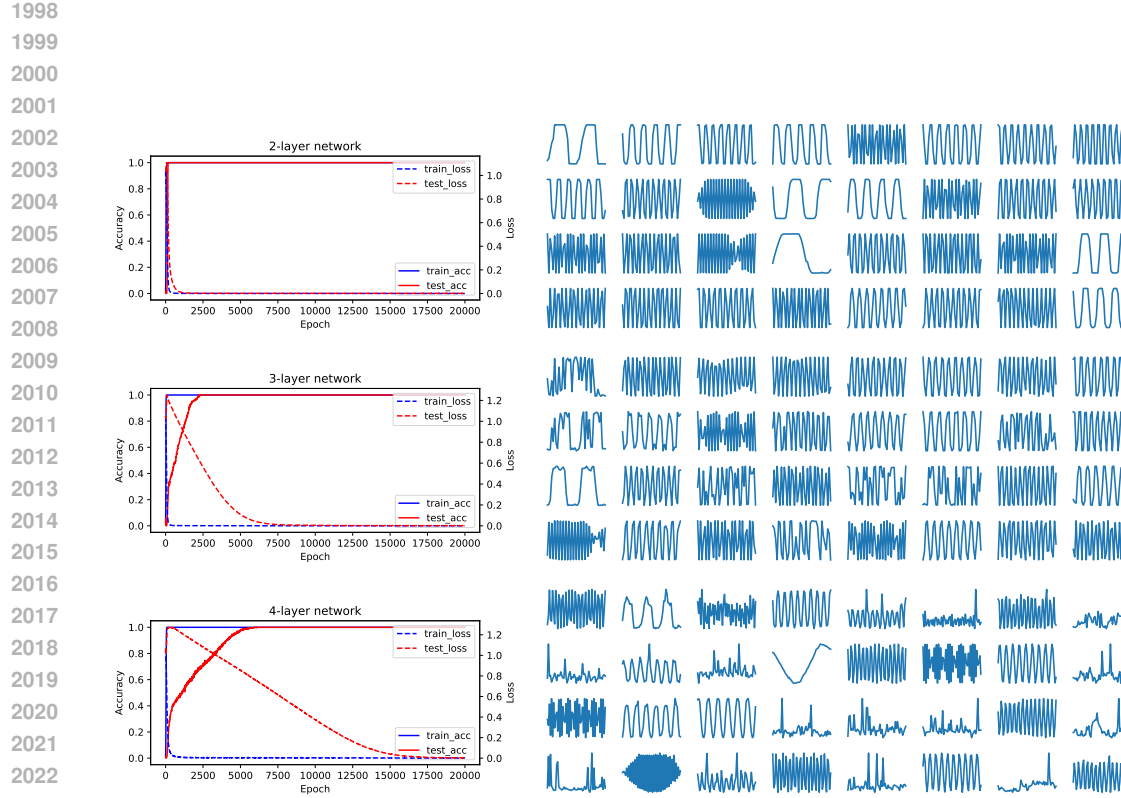


Figure 8: Training modular addition tasks with 2, 3 and 4 layer network with ReLU activations. **Left:** Training accuracy and losses. **Right:** Learned features at the lowest layer. With more layers, the training takes longer and grokking (delayed generalization) becomes more prominent. However, features at the lowest layer remain (distorted version) of Fourier bases, which are consistent with the analysis in Sec. 7.

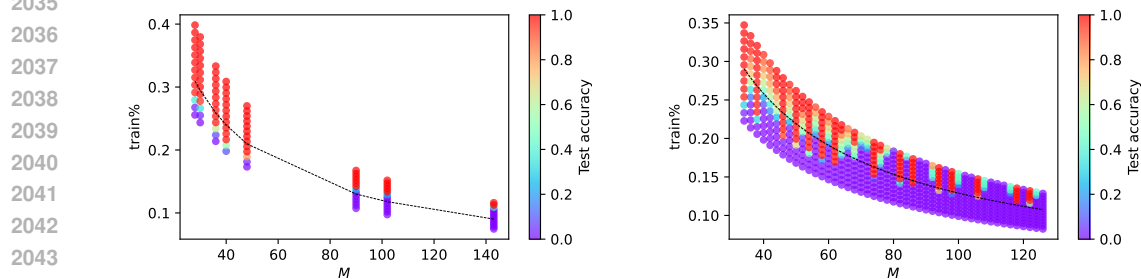


Figure 9: Generalization/memorization phase transition in product and non-Abelian tasks. **Left:** Product group $\mathbb{Z}_4 \otimes \mathbb{Z}_7$, $\mathbb{Z}_5 \otimes \mathbb{Z}_6$, $\mathbb{Z}_2 \otimes \mathbb{Z}_2 \otimes \mathbb{Z}_9$, $\mathbb{Z}_{13} \otimes \mathbb{Z}_{11}$, $\mathbb{Z}_5 \otimes \mathbb{Z}_2 \otimes \mathbb{Z}_2 \otimes \mathbb{Z}_2$, $\mathbb{Z}_6 \otimes \mathbb{Z}_4 \otimes \mathbb{Z}_2$, $\mathbb{Z}_3 \otimes \mathbb{Z}_2 \otimes \mathbb{Z}_{17}$, $\mathbb{Z}_2 \otimes \mathbb{Z}_3 \otimes \mathbb{Z}_3 \otimes \mathbb{Z}_5$. **Right:** Non-Abelian groups with $\max_k d_k = 2$ (maximal irreducible dimension 2). These non-Abelian groups are generated from GAP programs (See Appendix Sec. E.1).

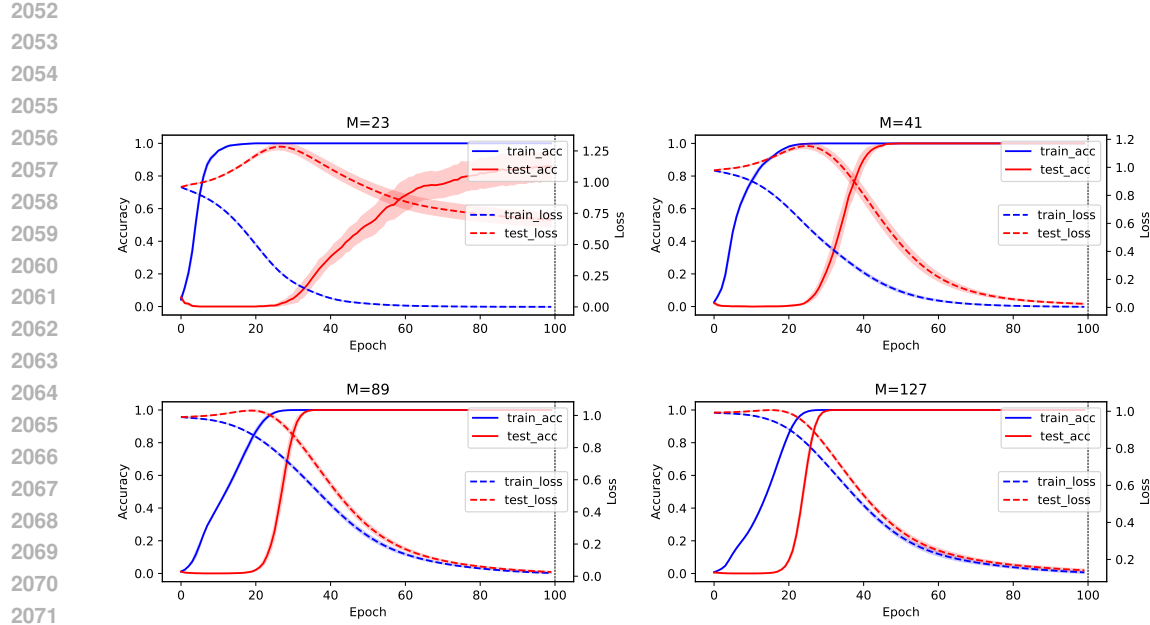


Figure 10: Training modular addition tasks with real weights ($M = 23, 41, 89, 127$). Learning rate is 0.005, weight decay is $5e - 5$. Number of hidden nodes $K = 256$. Test sample is 20% of the full set of M^2 . Using Adam optimizer. Averaged over 5 seeds. This is a baseline.

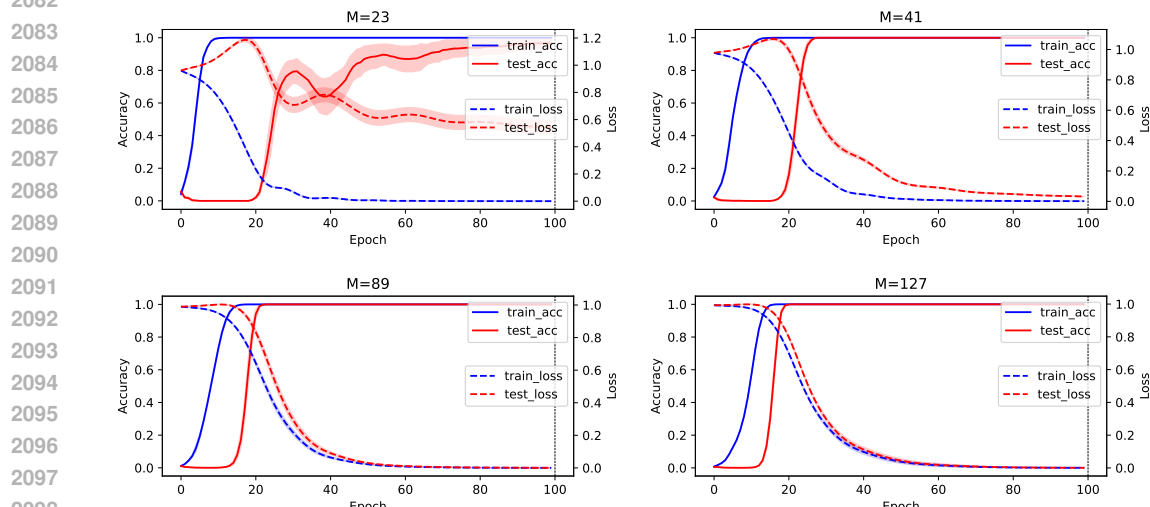


Figure 11: Training modular addition tasks with complex weights ($M = 23, 41, 89, 127$). Learning rate is 0.005, weight decay is $5e - 5$. Number of hidden nodes $K = 256$. Test sample is 20% of the full set of M^2 . Using Adam optimizer. Averaged over 5 seeds. Compared with the real case (Fig. 10), models with complex weights seem to grok faster.

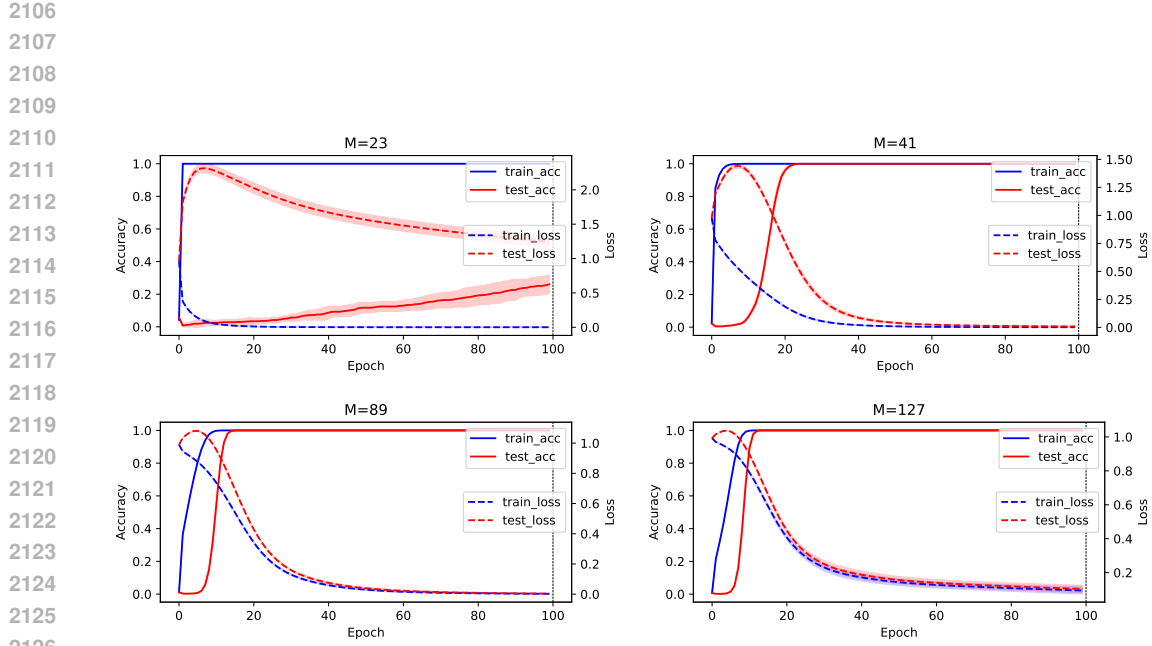


Figure 12: Training modular addition tasks with real weights ($M = 23, 41, 89, 127$). Instead of using gradient descent to update the top layer V , in every gradient update we use ridge regression solution V_{ridge} with respect to the current F (Eqn. ??). Learning rate is 0.005, weight decay is $5e - 5$. Number of hidden nodes $K = 256$. Test sample is 20% of the full set of M^2 . Using Adam optimizer. Averaged over 5 seeds. The grokking still happens (for $M = 23$ check Fig. 13 for completeness). It is slower for $M = 23$ but actually faster for $M = 41, 89, 127$, compared to the baseline (Fig. 10).

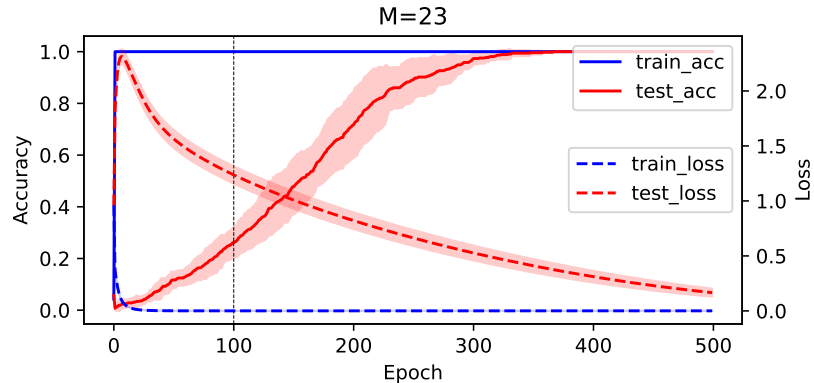


Figure 13: Training modular addition tasks with real weights $M = 23$ for 500 epochs, using V_{ridge} as the top layer weight. The grokking still happens but slower than the baseline (Fig. 10) for $M = 23$.